Journal of Inflammation Research

Dovepress
Taylor & Francis Group

Open Access Full Text Article

ORIGINAL RESEARCH

Siji Kangbingdu Mixture Ameliorates LPS-Induced Acute Lung Injury by Downregulating the TNF/IL-17 Signaling Pathways: A Comprehensive Study Using Transcriptomics, Network Pharmacology and Experimental Verification

Yuan Wang[1], Huiying Zhou[1], Bo Wang[2], Yuxi Liu[1], Kaihua Long[1], Hong Zhang[1]

[1]Institute of Chinese Materia Medica, Shaanxi Academy of Traditional Chinese Medicine (Shaanxi Provincial Hospital of Traditional Chinese Medicine), Xi'an, People's Republic of China; [2]College of Life Sciences, Northwest University, Xi'an, People's Republic of China

Correspondence: Kaihua Long; Hong Zhang, Shaanxi Academy of Traditional Chinese Medicine (Shaanxi Provincial Hospital of Traditional Chinese Medicine), No. 4 Xihuamen, Lianhu District, Xi'an, 710003, People's Republic of China, Email longkaihua@126.com; zhanghong919919@163.com

Background: Acute lung injury (ALI), as a respiratory condition triggered by various internal and external factors, is characterized clinically by high rates of incidence and mortality. In the current context where respiratory system diseases are on the rise, the incidence of ALI has been increasing annually. Previous research has established the efficacy of traditional Chinese medicine (TCM) in inhibiting ALI. Siji Kangbingdu Mixture (SJM), has demonstrated a clear clinical therapeutic effect in managing respiratory infections. Nevertheless, its mechanism of action in treating ALI is still lacking.

Purpose: To clarify the mechanism by which SJM exerts its therapeutic effects in the treatment of ALI.

Materials and Methods: In our study, we initially elucidated the chemical constituents of SJM by the UHPLC-Q-Orbitrap HRMS (LC-MS), and established an ALI model. Next, we evaluated how SJM inhibited ALI by measuring the weight curve of mice, the wet-to-dry lung weight ratio (W/D), the HE lung tissue pathological change score, along with the inflammatory factor expression. Then, by employing transcriptomics and network pharmacology approaches, the mechanism of SJM acting on ALI were predicted and analyzed. Finally, the expression and regulatory interactions of the differentially expressed target proteins in the key pathways were verified by qRT-PCR analysis, Western blotting (WB), immunofluorescence and immunohistochemistry.

Results: The LC-MS analysis identified 148 active ingredients. In vitro experiments indicated that SJM could significantly reduce the W/D index, pulmonary tissue pathological score, and the inflammatory factor levels. The findings from transcriptomics and network pharmacology suggested that SJM may alleviate ALI as a TNF and IL-17 signaling pathway. Further, through WB, immunofluorescence and immunohistochemistry, we noted significant downregulations in the pulmonary tissue expression of keys proteins in the SJM-H group.

Conclusion: SJM has the potential to inhibit the progression of ALI, and its mechanism of action may involve the TNF and IL-17 signaling downregulation.

Keywords: Siji kangbingdu mixture, acute lung injury, network pharmacology, transcriptomics, TNF signaling pathway, IL-17 signaling pathway

Introduction

Acute lung injury (ALI)/acute respiratory distress syndrome (ARDS) represents a dynamic process typified by lung edema and immediate inflammation[1] In recent years, despite extensive research concerning ALI, the mortality rate among ALI patients in the intensive care units remains alarmingly high, ranging from 40% to 60%.[2] Lipopolysaccharide (LPS), as a crucial cellular wall element for Gram-negative bacteria, can initiate the inherent immunity and inflict

Received: 27 August 2025
Accepted: 21 November 2025
Published: 30 December 2025

Graphical Abstract

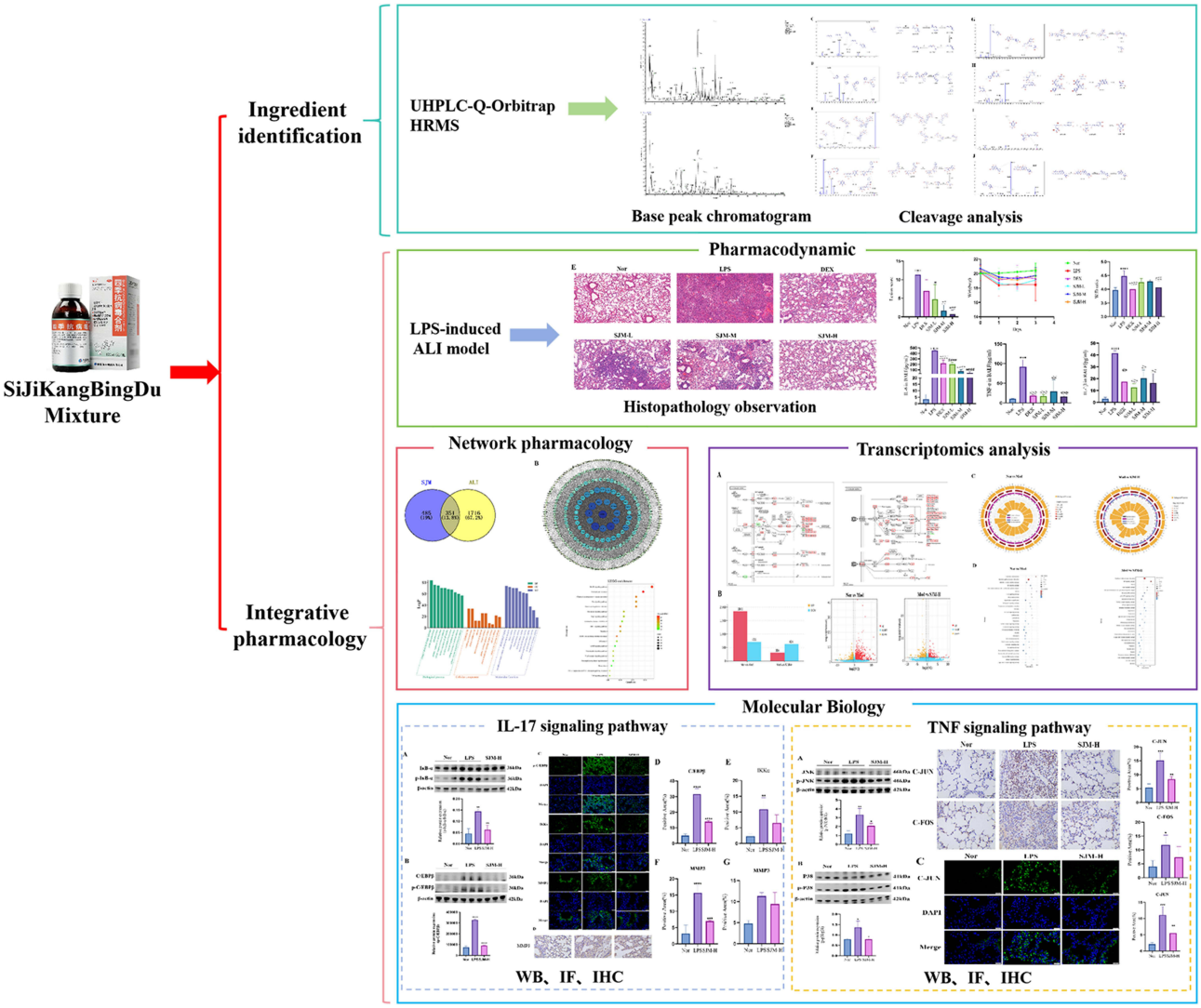

damage on the lung tissue.[3] When LPS is injected or enters the body through the trachea, it can induce microvascular lung injury, along with edema and inflammation of lung tissue, potentially even causing death[4] In our study, ALI was induced in mice through intratracheal instillation of LPS. The existing clinical therapeutic strategies for ALI can be categorized under supportive treatment and pharmaceutical intervention.[5] Mechanical ventilation has been shown to effectively improve the survival rate of ALI patients. Additionally, although symptomatic relief can be achieved through medications such as hormones and antioxidants, there is currently no specific pharmaceutical agent available for managing ALI.

The SJM formula is a modified and refined version of the Sangju Decoction and Yinqiao Powder as described in the "Treatise on Warm Diseases".[6] It contains 11 herbs, including *Schizonepeta tenuifolia* Briq. (Jingjie), *Platycodon grandiflorum (*Jacq.) A.DC. (Jiegeng), *Glycyrrhiza uralensis* Fisch. (Gancao), *Chrysanthemum morifolium* Ramat. (Juhua), *Perilla frutescens* (L.) Britt. (Zisuye), *Phragmites communis* Trin. (Lugen), *Mentha haplocalyx* Briq. (Bohe), *Forsythia suspensa* (Thunb.) Vahl (Lianqiao), *Houttuynia cordata* Thunb. (Yuxingcao), *Prunus armeniaca* L. var. *ansu* Maxim. (Kuxingren), *Morus alba* L. (Sangye). Among its ingredients, *Houttuynia cordata* Thunb.[7] *Forsythia suspensa* (Thunb.) Vahl,[8] and *Morus alba* L. are particularly efficacious in dispelling wind-heat, alleviating fever, removing toxins,

nourishing the lungs, suppressing cough, and soothing sore throat while reducing swelling. *Chrysanthemum morifolium* Ramat, *Prunus armeniaca* L. var. *ansu* Maxim. and *Platycodon grandiflorum* (Jacq.) A.DC. serve as the main ingredients for dispelling wind-heat, clearing the head and eyes, promoting the descent of lung qi, and alleviating cough by opening the orifices.[9] This is accompanied by *Perilla frutescens* (L.) Britt. and *Mentha haplocalyx* Briq. to induce sweating, relieve the exterior and expel pathogenic factors. *Perilla frutescens* (L). Britt. and *Phragmites communis* Trin. help promote the qi circulation, harmonize the middle jiao, generate body fluids and quench thirst. *Glycyrrhiza uralensis* Fisch. harmonizes various herbs in addition to enhancing lung function, alleviating cough, soothing sore throat, and eliminating phlegm. The combination of these herbs works synergistically to disperse wind, relieve exterior, clear heat, remove toxins, promote lung function and alleviate cough. SJM is commonly applied to individuals with upper airway infections, viral colds, influenza and other viral infectious diseases, who present symptoms such as headache, fever, runny nose and cough.[10] This TCM was produced by Shaanxi Haitian Pharmaceutical Co., Ltd, it has been used in clinical practice for more than twenty years and has received very positive feedback regarding its efficacy. This Chinese patent medicine is incorporated in the second trial version of the TCM Treatment Plan for the Novel Coronavirus-caused Pneumonia in Shaanxi, revised and finalized on January 31, 2020.[11] It is advised that 2019-nCoV-infected individuals use the SJM when exhibiting symptoms such as wind-cold attacking the exterior, along with qi deficiency and dampness stagnation, during the clinical treatment period.

In this investigation, we analyzed the bioactive constituents of SJM utilizing the ultra-performance liquid chromatography coupled with hybrid quadrupole orbitrap high resolution mass spectrometry (UHPLC-Q-Orbitrap HRMS) technique and elucidated the cleavage pathways of the representative chemical components. Moreover, the therapeutic efficacy of SJM against LPS-induced ALI in mice was investigated through network pharmacology and experimental inflammation methodologies. Finally, we performed a transcriptomic analysis of murine lung tissue and verified the mechanism by which SJM alleviates ALI using qRT-PCR, Western blotting, immunohistochemistry, and immunofluorescence.

Materials and Methods

Medicine and Reagents

The SJM was supplied by Haitian Pharmaceutical (XianYang, Shaanxi, China, Batch Number: 2404071), while Lipopolysaccharide (LPS, Batch number: 0000211692) was purchased from Sigma-Aldrich (United States). The IL-6 ELISA Kit (Catalog: E-EL-M0044), the TNF-α ELISA Kit (Catalog: E-EL-M3063) and the IL-1β ELISA Kit (Catalog: E-EL-M0037) utilized were all Elabscience Biotechnology products. Methanol (Grade: LC-MS/4 L; Article No. A456-4), Acetonitrile (Grade: LC-MS/4 L; Article No. A955-4), Formic acid (Grade: LC-MS/50 mL; Article No. A117-50). Antibodies against P-JNK (340,810), JNK (R24780), P-P38 (310,069), P38 (200,782), IκB-α (380,682), P-IκB-α (340,776), C/EBPβ (R380893), 1:750 dilutions, were procured from ZEN-BIOSCIENCE (Chengdu, China), whereas anti-P-C/EBPβ antibody (#AF3202), a 1:1000 dilution, was sourced from Affinity Biosciences.

Chemical Component Analysis

SJM sample (200 μL) and methanol (600 μL) were dispensed into a 1.5mL centrifuge tube for 30 minute of ultrasonication, after which an additional 10 minute centrifugation proceeded under 4°C and 12,000 rpm conditions. Then, an injection vial was pipetted with 100 μL of supernatant for detection purpose.

A Vanquish Flex UHPLC instrument (Thermo Fisher Scientific, MA, USA) was employed for the separation process, which was provided with an ACQUITY UHPLC HSS T3 column (1.7 μm, 2.1 mm ×100 mm; Waters, MA, USA). The mobile phases A and B were separately 0.1% formic acid in water and acetonitrile, with a flow rate set at 0.3 mL/min, while the column temperature was maintained at 40°C. Specifics on elution gradient were provided in Table 1, whereas the injection volume was set at 6.0 μL.

Table 1 Elution Gradient

Time (Min)	Mobile Phase	
	A (v%)	B (v%)
0	98	2
1.0	98	2
14.0	70	30
25.0	0	100
28.0	0	100
30.0	98	2

Animals and Model Establishment

Male C57 mice were acquired from Huachuang Cigna Pharmaceutical Technology (Jiangsu; certificate No. SCXK 2020–0009). The experimental protocols for animal studies received approval from the Ethics Committee of the Shaanxi Academy of TCM, under Animal Approval No. (2025–06). All procedures were conducted in strict compliance with the ARRIVE 2.0 Guidelines[12] The animal experiment protocol of this study strictly adheres to the Guidelines for the Ethical Review of Animal Welfare (GB/T 35892–2018). Prior to experimentation, the mice were acclimatized for 7 days under controlled conditions with 12-hour light and dark cycles. A power analysis was performed prior to the experiment to ensure adequate statistical power. Using G*Power with parameters set to $\alpha = 0.05$, power = 0.9, and a one-way ANOVA test, the analysis recommended a sample size of n = 9 per group. We therefore set our sample size to n = 10 per group to provide a buffer for any unexpected losses. A total of 60 male SPF C57 mice were used in this study, averaging 22 ± 2 g in weight, mice were group-housed (5 mice per cage) in standard ventilated polysulfone cages (330 x 215×170 mm), the cage is equipped with alamo wood shavings as bedding. The temperature should be maintained at 22 ± 1°C, and the humidity should be kept at 50 ± 5%, and provided standard animal feed and sufficient drinking water. 60 mice were used simple randomization method into six groups (10 in each group), experimental animal grouping and treatment regimen normal in Table 2, LPS (5 mg/kg), LPS + dexamethasone (DEX, 2 mg/kg), LPS + SJM-low (SJM-L, 3.85mL /kg), LPS + SJM-medium (SJM-M, 7.70mL/kg), and LPS + SJM-high (SJM-H, 15.4mL /kg). SJM and DEX were administered via gavage for 7 days, while the normal and LPS groups received saline. On the final day, all groups, barring the normal, were administered an intratracheal instillation of LPS 1.5 hours post-gavage.[13,14] The drug was administered continuously for 3 days after the model is established, and on the 10th day, the subsequent step involved euthanasia of mice with a pentobarbital sodium overdose, and cryopreservation of their bronchoalveolar lavage fluid (BALF), serum, and lung tissue at −80°C for later analyses. The mice that experienced weight loss 24 hours after LPS administration were selected as the inclusion criteria. To control for potential confounding effects of cage location within the animal room, all cages were rotated systematically every three days.

Table 2 Experimental Animal Grouping and Treatment Regimen

Group Name	Animal (n)	Treatment	Dose & Route of Administration	Frequency & Duration
Normal Group	10	Normal Saline	① Equivalent volume to LPS Group, intratracheal instillation	① Day 7
LPS Group	10	LPS	① 5mg/kg,intratracheal instillation	
Dexamethasone Group	10	LPS+dexamethasone	① 5mg/kg,intratracheal instillation ② Dexamethasone: 2 mg/kg, i.p.	① Day 7 ② Once daily, for 10 days
SJM-low Group	10	LPS+SJM-low dose	① 5mg/kg,intratracheal instillation ② SJM-low dose: 3.85mL /kg, P.O.	
SJM-medium Group	10	LPS+SJM-medium dose	① 5mg/kg,intratracheal instillation ② SJM-medium dose: 7.70mL/kg, P.O.	
SJM-high Group	10	LPS+SJM-high dose	① 5 mg/kg,intratracheal instillation ② SJM-high dose: 15.4mL /kg, P.O.	

Weight Curve and Status

During the murine modeling period, the changes in body weight, diet and water intake, as well as activity level of the mice were documented at 24, 48, and 72 hours post-modeling. Weight was the primary outcome measure for sample size calculation.

Wet-to-Dry Lung Weight Ratio (W/D)

The thoracic cavity of each mouse was opened and the left lung was excised. After separating the trachea and esophagus, the left lung lobe was weighed immediately to determine its wet mass. Following the euthanasia of the mice, the lungs were desiccated at 60°C for 72 hours until consistent weight was achieved, and the W/D index was subsequently calculated.[15]

Analysis of BALF Inflammatory Factors

After blood extraction, the mice were positioned on an operating table, their chest was opened, and their right lung was ligated. Pre-cooled PBS buffer (0.5 mL each rinse) was injected into the trachea, and the right lung was lavaged back and forth twice to collect BALF. The next step involved 15 minutes of sample centrifugation under 4°C and 3,000 rpm conditions. The resultant supernatant was examined using ELISA kits, following the respective instruction manuals, to assess the IL-6, TNF-α, and IL-1β expression.

Histopathological Changes of Lung Tissue

The lung tissue was immobilized using a 4% paraformaldehyde solution, dehydrated with a gradient of 75% ethanol, subjected to paraffin embedding, sliced post-cooling, stained by hematoxylin and eosin (H&E), and subsequently analyzed under a microscope after sealing.

Network Pharmacology

Acquisition of Component Targets and ALI Disease Targets

The bioactive components identified through LC-MS were imported one by one into the PubChem database to retrieve their SMILES codes. The corresponding gene targets for these components were acquired by utilizing the SwissTargetPrediction interface. In the GeneCards database, the disease targets were extracted by using the keyword "acute lung injury" after duplicate elimination.

Construction and Analysis of PPI Network

By importing the component and disease targets into Venny 2.1.0, the intersection targets were identified, which were then entered into the STRING repository to construct the protein-protein interaction (PPI) network. Utilizing Cytoscape 3.7.2, a visual network diagram of potential intersection targets was created, and the top ten core targets were selected according to their degree values.

GO and KEGG Enrichment Analyses

The component and disease intersection targets were analyzed for enriched Gene ontology (GO) functions alongside Kyoto Encyclopedia of Genes and Genomes (KEGG) pathways via Metascape (https://metascape.org/gp/index.html#/main/step1). The subsequent investigation was carried out from three dimensions, namely biological process (BP), cellular component (CC), and molecular function (MF) of the gene targets. Based on the top 10 results ranked by -LogP10 values, the GO functional results were visualized as a bar chart on the Microbial Informatics website (https://www.bioinformatics.com.cn). Meanwhile, based on P-value rankings, the top 20 signaling pathways were chosen from the KEGG result to create a bubble chart for visual analysis of the results.

Molecular Mechanism

qRT-PCR Analysis

The tissue of each mouse was lysed using Trizol, and total RNA from the serum was extracted for concentration assessment. Each sample was diluted, and subsequently reverse-transcribed into cDNA (condition: 20-μL reaction

Table 3 Primers Sequencing Used for mRNA Quantitation

Gene ID	Forward Primer Sequence	Reverse Primer Sequence
AKT1	5′-ATGAACGACGTAGCCATTGTG-3′	5′-TTGTAGCCAATAAAGGTGCCAT-3′
TNF	5′-CCCTCACACTCAGATCATCTTCT-3′	5′-GCTACGACGTGGGCTACAG-3′
IL-6	5′-TAGTCCTTCCTACCCCAATTTCC-3′	5′-TTGGTCCTTAGCCACTCCTTC-3′
MMP3	5′-ACATGGAGACTTTGTCCCTTTTG-3′	5′-TTGGCTGAGTGGTAGAGTCCC-3′
TP53	5'-CTCTCCCCCGCAAAAGAAAAA-3'	5'-CGGAACATCTCGAAGCGTTTA-3'

system). The qRT-PCR conditions: 30 seconds of pre-denaturation at 95°C, 10 seconds of denaturation at 95°C, 30 seconds of annealing and elongation at 60°C, with a total of 40 cycles conducted. The mRNA expression levels of AKT, TNF, IL-6, and MMP3 were quantified using the $2^{-\Delta\Delta Ct}$ method. The sequences are shown in Table 3.

Transcriptomic Analysis

The Trizol technique (Life Technologies) was utilized to isolate total RNA from pulmonary tissue, and agarose gel electrophoresis was undertaken to evaluate the quality of the extracted RNA. Transcriptome libraries were constructed using mRNA purification and fragmentation, succeeded by cDNA first-, second-strand syntheses, adapter ligation, and ligated product purification. The DNA 1000 Assay Kit (Agilent Technologies) was used for quality assessment. The DESeq2 in R software was applied to examine the expression of differential genes.

WB Analysis

The lung tissue was incorporated into RIPA buffer to create a homogenate. Following centrifugation, we collected the supernatant to measure the protein content by the BCA assay. Total protein was extracted via SDS-PAGE electrophoresis and subsequently shifted onto polyvinylidene fluoride membranes. Blockade in 5% BSA proceeded for a duration of 2 hours. Overnight probing was done using the primary antibodies. On the following day, the membranes underwent 2 hours of probing with secondary Goat Anti-Rabbit antibodies, after TBST rinsing, at ambient temperature. Finally, immunoreactive proteins were visualized using enhanced chemiluminescence.

Immunohistochemical Analysis

Antigen repair was performed on lung tissue samples after routine sectioning, dewaxing and rehydration. The samples were then blocked with 5% BSA, succeeded by an overnight probing at 4°C with primary antibody. Following the washing step, a fluorescent secondary antibody was introduced for an additional 1 hour probing at ambient temperature. After another round of washing, DAB was utilized for color development, the cell nuclei were re-stained by hematoxylin, and the cells were subsequently dehydrated and sealed. The final step involved observation and recording of the tissue section images under the microscope.

Immunofluorescence Analysis

Antigen repair was performed on lung tissue samples after routine sectioning, dewaxing and rehydration. The samples were then blocked with 5% BSA, followed by an overnight probing at 4°C with primary antibody. After the washing step, a fluorescent secondary antibody was introduced for an additional 1 hour probing at ambient temperature. After another round of washing, DAPI was added for core staining, and the anti-fluorescence quenching mounting agent was applied for mounting. The final step involved microscopic observation and recording of the tissue section images.

Statistical Analysis

GraphPad 10.0 was utilized to conduct all analyses. The data were expressed as the mean ± SD. ANOVA was applied for one-way analysis of variance among multiple groups, with differences considered statistically noteworthy when $P < 0.05$.

Results

Effective Chemical Components in SJM

In this study, UHPLC-Q-Orbitrap HRMS was employed for analysis, resulting in the identification of 148 active ingredients in SJM, which encompassed 31 glycosides, 14 terpenoids, 54 flavonoids, 10 lignans, 23 organic acids, 3 alkaloids and 13 other types. There were 82 chemical components in the positive ionic mode (Table 4) and 66 in the negative ionic mode (Table 5), with the chromatogram results illustrated in Figure 1.

SJM Alleviates ALI by Inhibiting Inflammatory Responses

After completing the "animal models and the treatment process" section (Figure 2A), we conducted the efficacy experiments of SJM. The ELISA analysis of BALF results indicated a marked upregulation in the inflammatory IL-6, TNF-α, and IL-1β in the LPS group versus the normal group (Figure 2B). The levels of these three inflammatory factors

Table 4 Identification of Chemical Constituents in SJM by the UHPLC-Q-Orbitrap HRMS (Positive Ion Mode)

No.	TR (min)	Identification	Formula	Classification	Ion mode	m/z		ppm (10–6)	Attribution
						Measured	Calculated		
1	0.82	L-glutamic acid	C5H9NO4	Carboxylic acids and derivatives	$[M+H]^+$	148.0604	148.0603	−0.98	abcdg
2	0.84	D-Sorbitol	C6H14O6	Organooxygen compounds	$[M+H]^+$	183.0863	183.0863	−0.15	b
3	0.84	L-carnitine	C7H15NO3	Organonitrogen compounds	$[M+H]^+$	162.1125	162.1123	−0.86	a
4	0.91	Adenine	C5H5N5	Imidazopyrimidines	$[M+H]^+$	136.0618	136.0618	−0.01	d
5	0.93	Stachyose	C24H42O21	Organooxygen compounds	$[M+NH4]^+$	684.2557	684.2557	0.03	abcg
6	3.96	Sophocarpine	C15H22N2O	Lupin alkaloids	$[M+H]^+$	247.1805	247.1804	−0.54	c
7	6.20	Salidroside	C14H20O7	Organooxygen compounds	$[M+NH4]^+$	318.1547	318.1544	−1.22	h
8	7.31	Vanillic acid	C8H8O4	Benzene and substituted derivatives	$[M+H]^+$	169.0495	169.0494	−1.08	efh
9	7.53	Cryptochlorogenic acid	C16H18O9	Organooxygen compounds	$[M+H]^+$	355.1024	355.1019	−1.20	dgi
10	7.59	Caffeic acid	C9H8O4	Cinnamic acids and derivatives	$[M+H]^+$	181.0495	181.0493	−1.29	abcdefghi
11	7.79	Amygdalin	C20H27NO11	Organooxygen compounds	$[M+NH4]^+$	475.1922	475.1920	−0.55	jk
12	7.95	Quercetin-3-rutinoside-7-glucoside	C33H40O21	Flavonoids	$[M+H]^+$	773.2135	773.2129	−0.70	a
13	8.90	Magnoflorine	C20H24NO4+	Aporphines	$[M]^+$	342.1700	342.1695	−1.57	g
14	9.41	Isovanilline	C8H8O3	Phenols	$[M+H]^+$	153.0546	153.0544	−1.24	a
15	9.52	Luteolin 7-diglucuronide	C27H26O18	Flavonoids	$[M+H]^+$	639.1192	639.1186	−0.94	e
16	9.52	p-Coumaric acid	C9H8O3	Cinnamic acids and derivatives	$[M+H]^+$	165.0546	165.0544	−1.12	afg
17	9.93	Vicenin III	C26H28O14	Flavonoids	$[M+H]^+$	565.1552	565.1547	−0.86	abcd
18	10.39	Vicenin I	C26H28O14	Flavonoids	$[M+H]^+$	565.1552	565.1546	−1.04	cd
19	10.70	Ferulic acid	C10H10O4	Cinnamic acids and derivatives	$[M+H-H2O]^+$	177.0546	177.0544	−1.32	aefgh
20	10.91	Vitexin	C21H20O10	Flavonoids	$[M+H]^+$	433.1129	433.1126	−0.86	bcd
21	11.00	Hyperoside	C21H20O12	Flavonoids	$[M+H]^+$	465.1028	465.1024	−0.84	dghi
22	11.00	Eriodictyol-7-O-glucoside	C21H22O11	Flavonoids	$[M+H]^+$	451.1235	451.1230	−1.03	ac
23	11.00	Calycosin-7-O-β-D-glucoside	C22H22O10	Isoflavonoids	$[M+H]^+$	447.1286	447.1282	−0.90	c
24	11.13	Kaempferol-3-O-glucorhamnoside	C27H30O15	Flavonoids	$[M+H]^+$	595.1657	595.1653	−0.83	agi
25	11.20	Forsythoside I	C29H36O15	Cinnamic acids and derivatives	$[M+NH4]^+$	642.2392	642.2383	−1.49	h
26	11.20	Scutellarin	C21H18O12	Flavonoids	$[M+H]^+$	463.0871	463.0866	−1.08	deg
27	11.28	Forsythoside A	C29H36O15	Cinnamic acids and derivatives	$[M+H]^+$	625.2127	625.2121	−1.00	h
28	11.50	Nicotiflorin	C27H30O15	Flavonoids	$[M+H]^+$	595.1657	595.1654	−0.51	agk

(*Continued*)

https://doi.org/10.2147/JIR.S562152

Table 4 (Continued).

No.	TR (min)	Identification	Formula	Classification	Ion mode	m/z		ppm (10–6)	Attribution
						Measured	Calculated		
29	11.52	Genistin	C21H20O10	Isoflavonoids	$[M+H]^+$	433.1129	433.1127	−0.49	c
30	11.80	Isochlorogenic acid A	C25H24O12	Organooxygen compounds	$[M+H]^+$	517.1341	517.1340	−0.04	cd
31	11.80	Perlolyrine	C16H12N2O2	Harmala alkaloids	$[M+H]^+$	265.0972	265.0968	−1.51	bd
32	11.93	Robinin	C33H40O19	Flavonoids	$[M+H-H2O]^+$	723.2131	723.2125	−0.85	d
33	12.11	Isochlorogenic acid B	C25H24O12	Organooxygen compounds	$[M+H-H2O]^+$	499.1235	499.1231	−0.82	dg
34	12.19	Apigenin-7-o-rutinoside	C27H30O14	Flavonoids	$[M+H]^+$	579.1708	579.1705	−0.60	g
35	12.30	(+)-Pinoresinol 4-O-glucoside	C26H32O11	Lignan glycosides	$[M+NH4]^+$	538.2283	538.2279	−0.66	bdh
36	12.38	Schizonepetoside B	C16H26O7	Pyranodioxins	$[M+NH4]^+$	348.2017	348.2010	−2.08	a
37	12.40	1-(3,4-Dihydroxyphenyl)-3-[2-(3,4-dihydroxyphenyl)-1-carboxy] ethoxycarbonyl-6,7-dihydroxy-1,2-dihydronaphthalene-2-carboxylic acid	C27H22O12	-	$[M+H-H2O]^+$	521.1078	521.1078	−0.11	g
38	12.75	Isochlorogenic acid C	C25H24O12	Organooxygen compounds	$[M+H]^+$	517.1341	517.1339	−0.39	cd
39	12.84	Diosmin	C28H32O15	Flavonoids	$[M+H]^+$	609.1814	609.1809	−0.86	cdg
40	12.86	Hesperetin 7-O-rutinoside	C28H34O15	-	$[M+H]^+$	611.1970	611.1963	−1.22	d
41	12.88	Eriodictiol-7-glucoside	C22H24O11	Flavonoids	$[M+H]^+$	465.1391	465.1390	−0.31	a
42	13.16	Luteolin-7-O-beta-D-glucuronide	C21H18O12	Flavonoids	$[M+H]^+$	463.0871	463.0869	−0.53	e
43	13.42	Scoparone	C11H10O4	Coumarins and derivatives	$[M+H]^+$	207.0652	207.0650	−1.09	h
44	13.51	Isoliquiritin apioside	C26H30O13	Flavonoids	$[M+H]^+$	551.1759	551.1755	−0.83	c
45	13.57	Matairesinoside	C26H32O11	Lignan glycosides	$[M+H]^+$	521.2017	521.2015	−0.50	h
46	14.06	Ononin	C22H22O9	Isoflavonoids	$[M+H]^+$	431.1337	431.1335	−0.47	c
47	14.19	Isoliquiritin	C21H22O9	Flavonoids	$[M+H]^+$	419.1337	419.1332	−1.19	ac
48	14.30	6-p-methoxycinnamoyl catalpol	C25H30O12	Organooxygen compounds	$[M+H]^+$	523.1810	523.1807	−0.66	dj
49	14.45	Schizonol	C10H16O2	Prenol lipids	$[M+H-H2O]^+$	151.1117	151.1115	−1.20	a
50	14.89	Platycodin D3	C63H102O33	Prenol lipids	$[M+H]^+$	1387.6376	1387.6377	0.03	b
51	14.89	Platycoside L	C42H68O17	Prenol lipids	$[M+H]^+$	845.4529	845.4514	−1.76	b
52	15.06	Phillyrin	C27H34O11	Lignan glycosides	$[M+NH4]^+$	552.2439	552.2436	−0.62	h
53	15.49	Didymin	C28H34O14	Flavonoids	$[M+H]^+$	595.2021	595.2018	−0.62	ag
54	15.88	Iristectorigenin A	C17H14O7	Isoflavonoids	$[M+H-H2O]^+$	313.0707	313.0699	−2.24	k
55	16.01	(-)-Syringaresinol	C22H26O8	Furanoid lignans	$[M+H-H2O]^+$	401.1595	401.1591	−0.96	abcdg
56	16.21	Deapio-Platycodin-D	C52H84O24	Prenol lipids	$[M+H]^+$	1093.5425	1093.5412	−1.26	b
57	16.45	Platycoside K	C42H68O17	Prenol lipids	$[M+H]^+$	845.4529	845.4514	−1.85	b
58	16.80	Echinatin	C16H14O4	Linear 1,3-diarylpropanoids	$[M+H]^+$	271.0965	271.0959	−2.32	c
59	16.87	Cinerolon	C10H14O2	Organooxygen compounds	$[2M+H]^+$	333.2060	333.2054	−1.87	a
60	16.89	3-o-β-d-glucopyranosyl platycodigenin	C36H58O12	Prenol lipids	$[M+H]^+$	683.4001	683.3992	−1.31	b
61	17.09	Licoricesaponin a3	C48H72O21	Prenol lipids	$[M+H]^+$	985.4639	985.4622	−1.69	c
62	17.34	Matairesinol	C20H22O6	Furanoid lignans	$[M+H]^+$	359.1489	359.1483	−1.75	h j
63	17.51	Platycodigenin	C30H48O7	Prenol lipids	$[M+H-H2O]^+$	503.3367	503.3363	−0.82	b
64	17.67	Platycogenic acid A	C30H46O8	Prenol lipids	$[M+H-H2O]^+$	517.3160	517.3156	−0.66	b
65	18.26	(-)-Perillaldehyde	C10H14O	Prenol lipids	$[M+H]^+$	151.1117	151.1115	−1.61	e
66	18.37	Arctigenin	C21H24O6	Furanoid lignans	$[M+H]^+$	373.1646	373.1639	−1.69	h
67	18.46	Polygalacic acid	C30H48O6	Prenol lipids	$[M+H-H2O]^+$	487.3418	487.3413	−1.02	b
68	18.48	Glycyrrhizic acid	C42H62O16	Prenol lipids	$[M+H]^+$	823.4111	823.4097	−1.67	c
69	18.95	Pinellic acid	C18H34O5	Fatty Acyls	$[M+H-H2O]^+$	313.2373	313.2365	−2.47	e
70	18.97	Soyasaponin Bb	C48H78O18	Prenol lipids	$[M+H]^+$	943.5261	943.5249	−1.31	c
71	19.08	Eupatorin	C18H16O7	Flavonoids	$[M+H]^+$	345.0969	345.0962	−1.93	d
72	19.26	Licorice-saponin j2	C42H64O16	Prenol lipids	$[M+H]^+$	825.4267	825.4244	−2.82	c
73	19.39	Casticin	C19H18O8	Flavonoids	$[M+H]^+$	375.1074	375.1069	−1.52	d
74	19.59	Gancaonin b	C21H20O6	Isoflavonoids	$[M+H]^+$	369.1333	369.1326	−1.81	c
75	19.64	Licoricesaponin b2	C42H64O15	Prenol lipids	$[M+NH4]^+$	826.4583	826.4571	−1.51	c

(*Continued*)

Table 4 (Continued).

No.	TR (min)	Identification	Formula	Classification	Ion mode	m/z		ppm (10–6)	Attribution
						Measured	Calculated		
76	19.81	Semilicoisoflavone b	C20H16O6	Isoflavonoids	$[M+H]^+$	353.1020	353.1012	−2.12	c
77	20.13	Glyasperin f	C20H18O6	Isoflavonoids	$[M+H]^+$	355.1176	355.1170	−1.73	c
78	20.15	Pulegone	C10H16O	Prenol lipids	$[M+H]^+$	153.1274	153.1272	−1.56	aegjk
79	20.44	Glycyrrhetic acid 3-O-β-D-glucuronide	C36H54O10	Prenol lipids	$[M+H]^+$	647.3790	647.3783	−1.03	c
80	20.50	Asperglaucide	C27H28N2O4	Carboxylic acids and derivatives	$[M+H]^+$	445.2122	445.2118	−0.82	af
81	20.59	Artemetin	C20H20O8	Flavonoids	$[M+H]^+$	389.1231	389.1225	−1.41	bdf
82	23.33	Pulsatillic acid	C30H46O4	Prenol lipids	$[M+H]^+$	471.3469	471.3466	−0.51	ak

Notes: a:Schizonepeta tenuifolia Briq. b: Platycodon grandiflorum (Jacq.) A.DC. c: Glycyrrhiza uralensis Fisch. d: Chrysanthemum morifolium Ramat. e: Perilla frutescens (L.) Britt. f: Phragmites communis Trin. g: Mentha haplocalyx Briq. h: Forsythia suspensa (Thunb.) Vahl i: Houttuynia cordata Thunb. j: Prunus armeniaca L.var.ansu Maxim. k: Morus alb L.

Table 5 Identification of Chemical Constituents in SJM by the UHPLC-Q-Orbitrap HRMS (Negative Ion Mode)

No.	TR (min)	Identification	Formula	Classification	Ion mode	m/z		ppm (10–6)	Attribution
						Measured	Calculated		
1	0.84	(+)-Quinic acid	C7H12O6	-	$[M+FA-H]^-$	237.0616	237.0607	−4.65	i
2	0.88	1-Kestose	C18H32O16	Organooxygen compounds	$[M+FA-H]^-$	549.1672	549.1670	−0.53	abcdg
3	0.91	Sucrose	C12H22O11	Organooxygen compounds	$[M+FA-H]^-$	387.1144	387.1143	−0.48	ck
4	0.91	Maltopentaose	C30H52O26	Organooxygen compounds	$[M-H]^-$	827.2674	827.2670	−0.49	g
5	1.23	Panose b	C18H32O16	Organooxygen compounds	$[M+FA-H]^-$	549.1672	549.1671	−0.23	k
6	1.26	Nystose	C24H42O21	Organooxygen compounds	$[M+FA-H]^-$	711.2201	711.2194	−0.96	b
7	5.50	Neochlorogenic acid	C16H18O9	Organooxygen compounds	$[M-H]^-$	353.0878	353.0878	−0.11	dghi
8	5.50	Adoxosidic acid	C16H24O10	Prenol lipids	$[2M-H]^-$	751.2666	751.2668	0.30	h
9	5.89	4-Hydroxybenzoic acid	C7H6O3	Benzene and substituted derivatives	$[2M-H]^-$	275.0561	275.0562	0.47	f
10	7.17	Chlorogenic acid	C16H18O9	Organooxygen compounds	$[M-H]^-$	353.0878	353.0879	0.19	dghijk
11	7.58	Caffeate	C9H8O4	Cinnamic acids and derivatives	$[2M-H]^-$	359.0772	359.0773	0.07	h
12	7.87	Myricetin-3-rutinoside	C27H30O17	Flavonoids	$[M-H]^-$	625.1410	625.1413	0.46	a
13	8.37	(z)-8-β-d-glucopyranosyloxycinnamicacid	C15H18O8	Fatty Acyls	$[M-H]^-$	325.0929	325.0930	0.48	a
14	8.75	5-p-cis-coumaroylquinicacid	C16H18O8	Organooxygen compounds	$[M-H]^-$	337.0929	337.0932	0.94	a
15	8.95	Vicenin 2	C27H30O15	Flavonoids	$[M-H]^-$	593.1512	593.1512	0.01	cdg
16	9.02	Prunasin	C14H17NO6	Organooxygen compounds	$[M+FA-H]^-$	340.1038	340.1035	−0.83	ej
17	9.51	Forsythoside C	C29H36O16	Cinnamic acids and derivatives	$[M+FA-H]^-$	685.1985	685.1992	1.04	h
18	9.53	4-O-Feruloylquinic acid	C17H20O9	Organooxygen compounds	$[M-H]^-$	367.1035	367.1034	−0.27	g
19	9.87	Rengyoside C	C22H32O10	Organooxygen compounds	$[M+FA-H]^-$	501.1977	501.1979	0.29	h
20	9.92	Schaftoside	C26H28O14	Flavonoids	$[M-H]^-$	563.1406	563.1406	−0.08	abcd
21	10.23	Schizonepetoside C	C16H26O7	Organooxygen compounds	$[M+FA-H]^-$	375.1661	375.1662	0.43	a
22	10.44	Calceolarioside A	C23H26O11	Cinnamic acids and derivatives	$[M-H]^-$	477.1402	477.1403	0.15	h
23	10.51	Apigenin-7-o-diglucuronide	C27H26O17	Flavonoids	$[M-H]^-$	621.1097	621.1102	0.83	e

(*Continued*)

https://doi.org/10.2147/JIR.S562152

Table 5 (Continued).

No.	TR (min)	Identification	Formula	Classification	Ion mode	m/z		ppm (10–6)	Attribution
						Measured	Calculated		
24	10.66	Calceolarioside C	C28H34O15	Cinnamic acids and derivatives	$[M-H]^-$	609.1825	609.1825	0.06	h
25	10.87	Rutin	C27H30O16	Flavonoids	$[M-H]^-$	609.1461	609.1466	0.83	dghik
26	10.89	Liquiritin	C21H22O9	Flavonoids	$[M-H]^-$	417.1191	417.1191	−0.12	cj
27	10.94	Liquiritin apioside	C26H30O13	Flavonoids	$[M-H]^-$	549.1614	549.1611	−0.46	c
28	10.96	Luteolin-7-o-rutinoside	C27H30O14	Flavonoids	$[M-H]^-$	577.1563	577.1561	−0.31	dgj
29	11.27	Forsythoside H	C29H36O15	Cinnamic acids and derivatives	$[M+FA-H]^-$	669.2036	669.2032	−0.71	h
30	11.38	Cynaroside	C21H20O11	Flavonoids	$[M-H]^-$	447.0933	447.0935	0.43	adeg
31	12.08	Lobetyolinin	C26H38O13	Fatty Acyls	$[M+FA-H]^-$	603.2294	603.2302	1.34	b
32	12.26	Lipedoside A	C29H36O14	Cinnamic acids and derivatives	$[M-H]^-$	607.2032	607.2036	0.66	h
33	12.35	Quercitrin	C21H20O11	Flavonoids	$[M-H]^-$	447.0933	447.0934	0.22	di
34	12.58	Apigenin-7-glucoside	C21H20O10	Flavonoids	$[M-H]^-$	431.0984	431.0984	0.17	acde
35	12.60	Apigenin-7-glucuronide	C21H18O11	Flavonoids	$[M-H]^-$	445.0776	445.0777	0.05	d
36	12.72	(+)-Phylliroside	C27H34O11	Lignan glycosides	$[M+FA-H]^-$	579.2083	579.2086	0.49	h
37	12.81	(+)-Epipinoresinol-4′-O-D-glucoside	C26H32O11	Lignan glycosides	$[M+FA-H]^-$	565.1927	565.1927	0.06	h
38	12.86	Hesperidin	C28H34O15	Flavonoids	$[M-H]^-$	609.1825	609.1824	−0.12	adg
39	12.88	Rosmarinic acid	C18H16O8	Cinnamic acids and derivatives	$[M-H]^-$	359.0772	359.0773	0.21	aeg
40	13.10	Lithospermic acid	C27H22O12	2-arylbenzofuran flavonoids	$[M-H]^-$	537.1038	537.1044	1.06	a
41	13.31	Diosmetin-7-O-β-D-glucopyranoside	C22H22O11	Flavonoids	$[M+FA-H]^-$	507.1144	507.1144	−0.06	cdg
42	13.44	(2S)-2-[(1S,2R)-3-[(1S)-1-Carboxy-2-(3,4-dihydroxyphenyl)ethoxy]carbonyl-2-(3,4-dihydroxyphenyl)-7,8-dihydroxy-1,2-dihydronaphthalene-1-carbonyl]oxy-3-(3,4-dihydroxyphenyl)propanoic acid	C36H30O16	Naphthalenes	$[M-H]^-$	717.1461	717.1474	1.74	g
43	13.83	Salvianolic acid B	C36H30O16	2-arylbenzofuran flavonoids	$[M-H]^-$	717.1461	717.1471	1.43	ab
44	13.83	Licuraside	C26H30O13	Flavonoids	$[M-H]^-$	549.1614	549.1619	0.92	c
45	14.48	Liquiritigenin	C15H12O4	Flavonoids	$[M-H]^-$	255.0663	255.0661	−0.74	c
46	14.48	Forsythin	C27H34O11	Lignan glycosides	$[M+FA-H]^-$	579.2083	579.2087	0.71	h
47	14.48	Licochalcone B	C16H14O5	Linear 1,3-diarylpropanoids	$[M-H]^-$	285.0768	285.0769	0.34	cgj
48	14.66	Deapio-Platycodin-D3	C58H94O29	Prenol lipids	$[M+FA-H]^-$	1299.5863	1299.5872	0.76	b
49	15.31	Buddleoside	C28H32O14	Flavonoids	$[M+FA-H]^-$	637.1774	637.1782	1.40	dg
50	15.33	Platycoside G3	C63H102O32	Prenol lipids	$[M+FA-H]^-$	1415.6336	1415.6350	0.99	b
51	16.06	Tilianine	C22H22O10	Flavonoids	$[M+FA-H]^-$	491.1195	491.1195	−0.01	ad
52	16.10	Platycoside A	C58H94O29	Prenol lipids	$[M-H]^-$	1253.5808	1253.5799	−0.70	b
53	16.30	Platycodin D2	C63H102O33	Prenol lipids	$[M-H]^-$	1385.6231	1385.6223	−0.56	b
54	16.39	Platycodin D	C57H92O28	Prenol lipids	$[M-H]^-$	1223.5702	1223.5688	−1.14	b
55	16.41	Polygalacin D2	C63H102O32	Prenol lipids	$[M-H]^-$	1369.6281	1369.6268	−0.96	b
56	16.55	Polygalacin D	C57H92O27	Prenol lipids	$[M-H]^-$	1207.5753	1207.5751	−0.17	b
57	16.56	Platyconic acid A	C57H90O29	Prenol lipids	$[M-H]^-$	1237.5495	1237.5493	−0.19	b
58	16.90	3″O-Acetylplatycodin D	C59H94O29	Prenol lipids	$[M-H]^-$	1265.5808	1265.5800	−0.60	b
59	17.04	3″-O-Acetylpolygalacin D	C59H94O28	-	$[M-H]^-$	1249.5859	1249.5855	−0.32	b
60	17.28	Apigenin	C15H10O5	Flavonoids	$[M-H]^-$	269.0455	269.0456	0.21	adeg
61	17.82	Isoliquiritigenin	C15H12O4	Linear 1,3-diarylpropanoids	$[M-H]^-$	255.0663	255.0660	−1.06	acj
62	18.02	Licoricesaponin e2	C42H60O16	Prenol lipids	$[M-H]^-$	819.3809	819.3819	1.23	c
63	18.16	Formononetin	C16H12O4	Isoflavonoids	$[M-H]^-$	267.0663	267.0662	−0.13	c
64	18.92	Liquorice	C42H62O16	Prenol lipids	$[M-H]^-$	821.3965	821.3975	1.20	j
65	19.32	Apioglycyrrhizin	C41H62O14	Prenol lipids	$[M-H]^-$	777.4067	777.4075	1.09	c
66	19.47	Licoricesaponine c2	C42H62O15	Prenol lipids	$[M-H]^-$	805.4016	805.4027	1.36	c

Notes: a:Schizonepeta tenuifolia Briq. b: Platycodon grandiflorum (Jacq.) A.DC. c: Glycyrrhiza uralensis Fisch. d: Chrysanthemum morifolium Ramat. e: Perilla frutescens (L.) Britt. f: Phragmites communis Trin. g: Mentha haplocalyx Briq. h: Forsythia suspensa (Thunb.) Vahl i: Houttuynia cordata Thunb. j: Prunus armeniaca L.var.ansu Maxim. k: Morus alba L.

in each SJM administration group decreased significantly relative to the LPS group. This finding suggests that SJM may ameliorate the inflammatory response within lung tissue.

During the modeling process of mice with ALI, the model group exhibited reduced autonomous activity, diminished food and water intake, breathing difficulties, as well as more secretions at the corners of the eyes when compared to the normal group. After 24 hours of LPS administration, the body weight of the mice showed a downward trend. The administration groups showed improvement in the physical sign status relative to the LPS group, with increased autonomous activity and the status approaching that of the normal group. After 24 hours of modeling, the model mice displayed a reduction in body weight relative to the normal group, while the SJM administration and DEX groups exhibited a body weight increase relative to the model group. At 72 hours of modeling, an upward trend in body weight was noted with the SJM administration groups (Figure 2C). The LPS group demonstrated a significantly elevated W/D index, while the W/D index of the SJM-H group decreased significantly in comparison to the LPS group (Figure 2D).

The pulmonary tissue structure for the blank mice displayed no abnormalities, the contours of alveoli and chambers were intact and clear, and no signs of hemorrhage, edema or inflammatory cell infiltration were observed. In contrast, the model mice exhibited a disordered pulmonary tissue structure, with altered alveolar structures, congested capillaries, edematous and hemorrhagic tissue, and presence of inflammatory cell infiltration, suggesting considerable damage to the pulmonary tissue. The tissue lesions in the SJM-H showed marked improvement in comparison to the model group, with

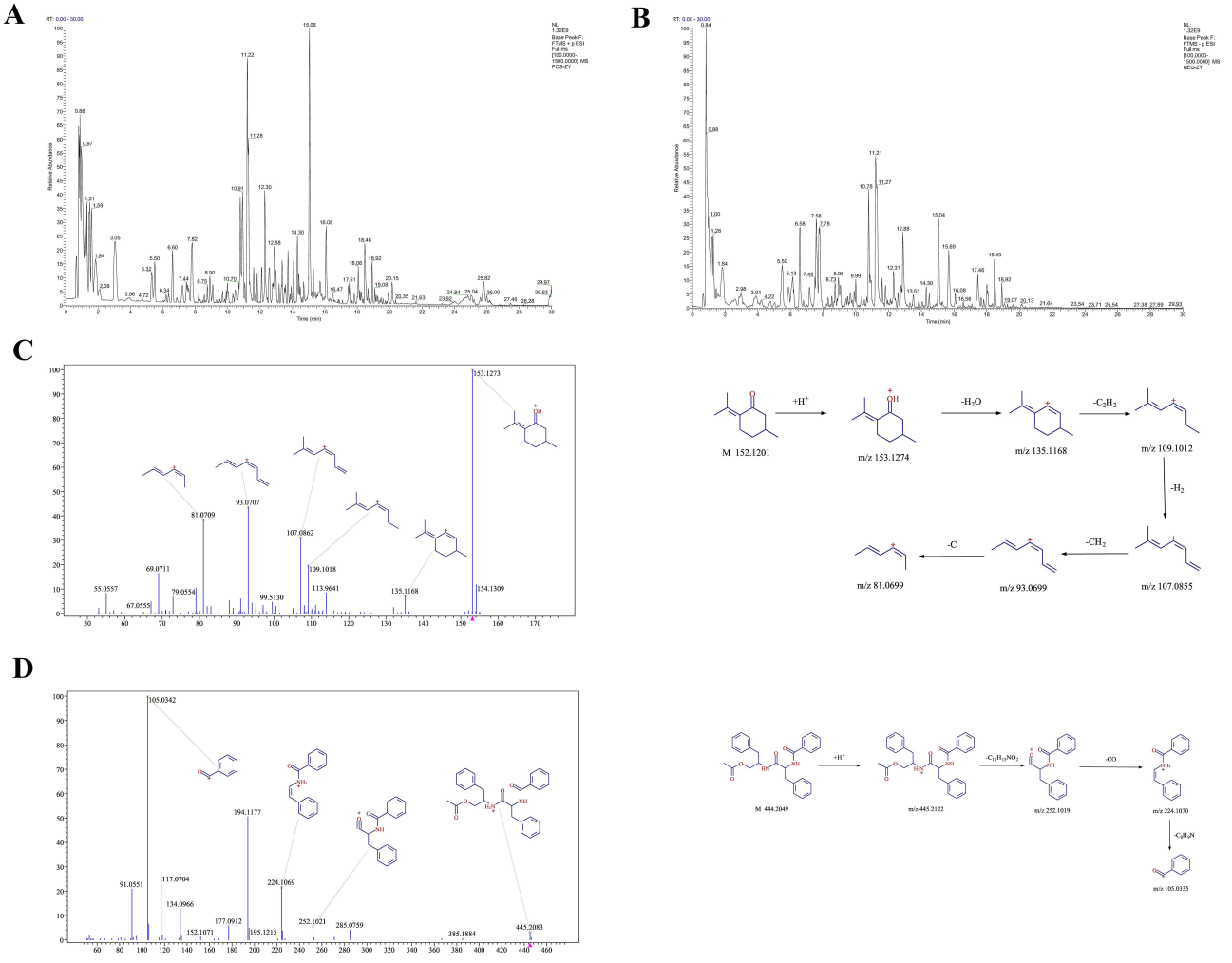

Figure 1 Continued.

https://doi.org/10.2147/JIR.S562152

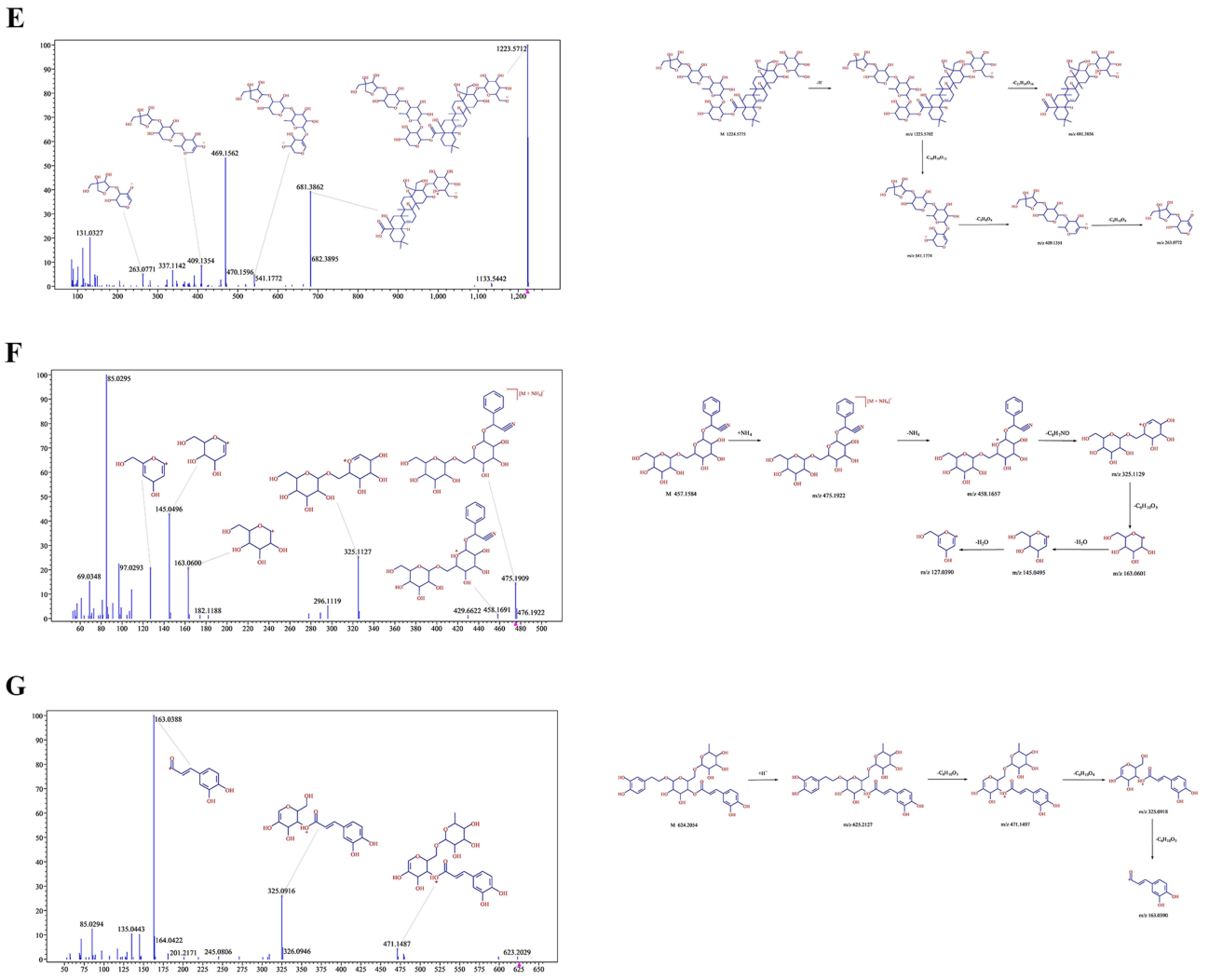

Figure 1 Continued.

a restoration trend of alveolar structure, and an effectively alleviated inflammatory cell infiltration in the pulmonary interstitium (Figure 2E and F).

Network Pharmacology Analysis

From the SwissTargetPrediction database, 836 targets were obtained. Using the GeneCards disease genes list, 2,067 targets associated with ALI were identified. The intersection of these two target sets was calculated, yielding 351 common targets, which were predicted to be the relevant targets for treating ALI (Figure 3A). A "tsv" format file was generated by uploading these intersection targets to the STRING repository. Cytoscape 3.7.2 was utilized to draw the PPI network diagram illustrating the intersection of SJM and ALI targets, resulting in 9,677 edges and 350 nodes. Among them, the top 10 core targets based on degree value were GAPDH, AKT1, TP53, TNF, IL6, EGFR, STAT3, BCL2, CASP3, and HIF1A (Figure 3B). The intersection targets were then imported into Metascape for enrichment analyses. The GO functional analysis produced 3,509 results, comprising 2,957 in BP, 389 in MF, and 163 in CC. The KEGG enrichment results revealed 223 pathways, among which the primary pathway involved in inflammatory response and oxidative stress was the MAPK signaling pathway (Figures 3C and D). Additionally, we conducted a qRT-PCR experiment to verify the key proteins obtained from the PPIs. The findings indicated that SJM-H could notably

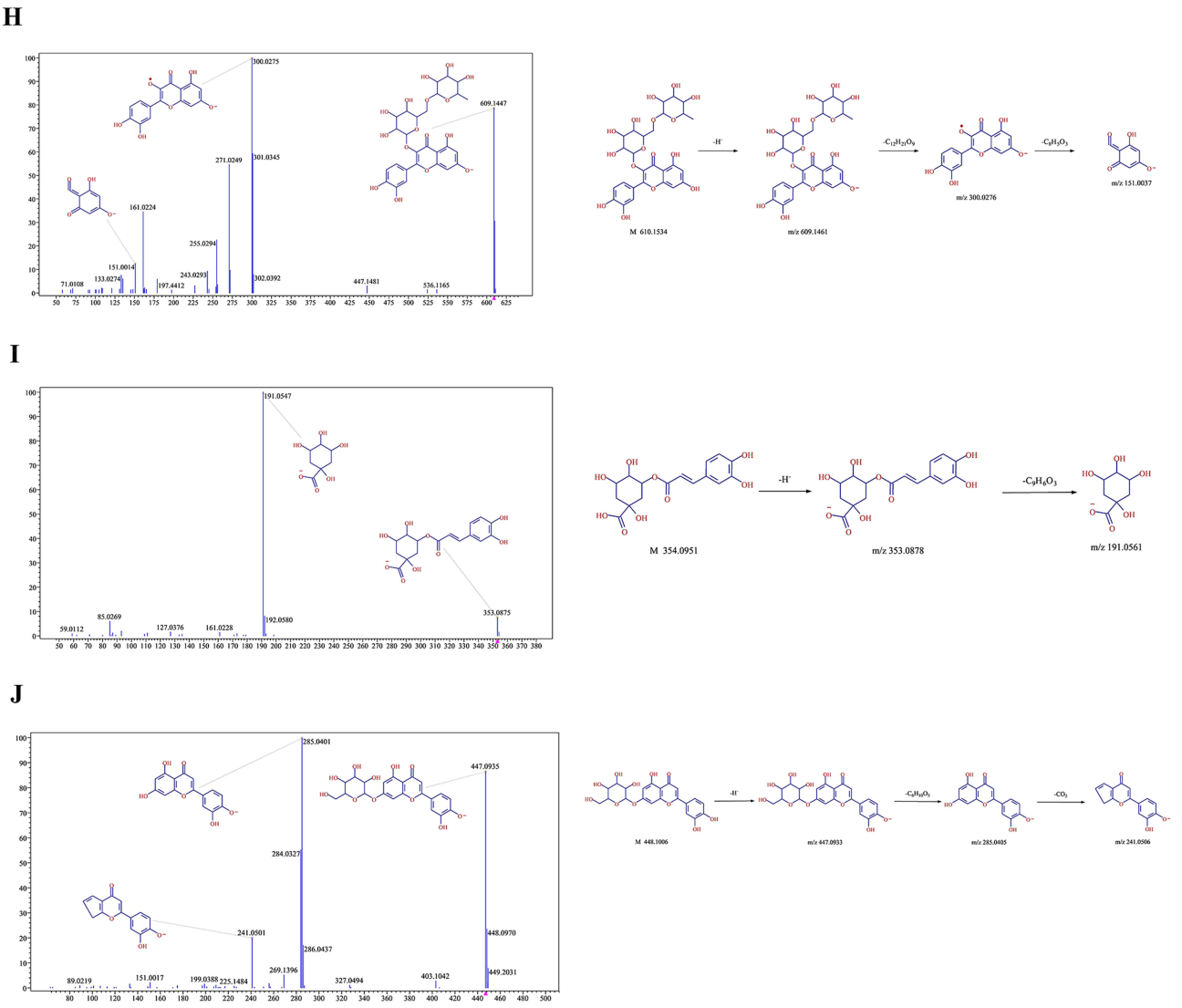

Figure 1 The chromatogram of the SJM and The chemical structure of the representative component. (**A**) Chromatogram in the positive ion mode. (**B**) Chromatogram in negative ion mode. (**C**) The decomposition pattern diagram and the diagram marking the secondary fragments of Pulegone. (**D**) The decomposition pattern diagram and the diagram marking the secondary fragments of Asperglaucide. (**E**) The decomposition pattern diagram and the diagram marking the secondary fragments of Platycodin D. (**F**) The decomposition pattern diagram and the diagram marking the secondary fragments of Amygdalin. (**G**) The decomposition pattern diagram and the diagram marking the secondary fragments of Forsythoside A. (**H**) The decomposition pattern diagram and the diagram marking the secondary fragments of Rutin. (**I**) The decomposition pattern diagram and the diagram marking the secondary fragments of Chlorogenic acid. (**J**) The decomposition pattern diagram and the diagram marking the secondary fragments of Cynaroside.

downregulate the AKT, IL-6, TNF, MMP3, and TP53 mRNA expression in the lung tissue relative to the LPS group (Figure 3E).

Transcriptomic Analysis in SJM

Initially, the differential genes among the samples were compared. In the LPS group, a total of 2,552 differential genes were screened out compared with the normal group, among which 1,841 were upregulated and 711 were downregulated. The SJM-H group revealed 928 differential genes compared to the LPS group, with 304 being upregulated and 624 being downregulated. The differential genes from the normal, LPS and SJM-H groups underwent further cluster analysis to produce the volcano map. The results indicated significant disparities in gene expression between the normal group and the model group, as well as between the model group and the LPS group versus the SJM-H group, demonstrating good

distinctions among the groups (Figure 4B). Further, the BP in GO functional analysis primarily involved cellular processes, biological regulation, and regulation of biological processes. The MF chiefly involved catalytic activities, binding, and regulation of molecular functions. The CC mainly designed the protein-containing complexes alongside cellular anatomical entities (Figure 4C). Intergroup differential genes were subjected to KEGG enrichment analysis. The differential genes between the normal versus LPS group primarily involved NOD-like receptor, TNF, and IL-17 signaling pathways, while those between the LPS versus SJM-H group mainly involved TNF, IL-17, and JAK-STAT signaling pathways (Figure 4D).

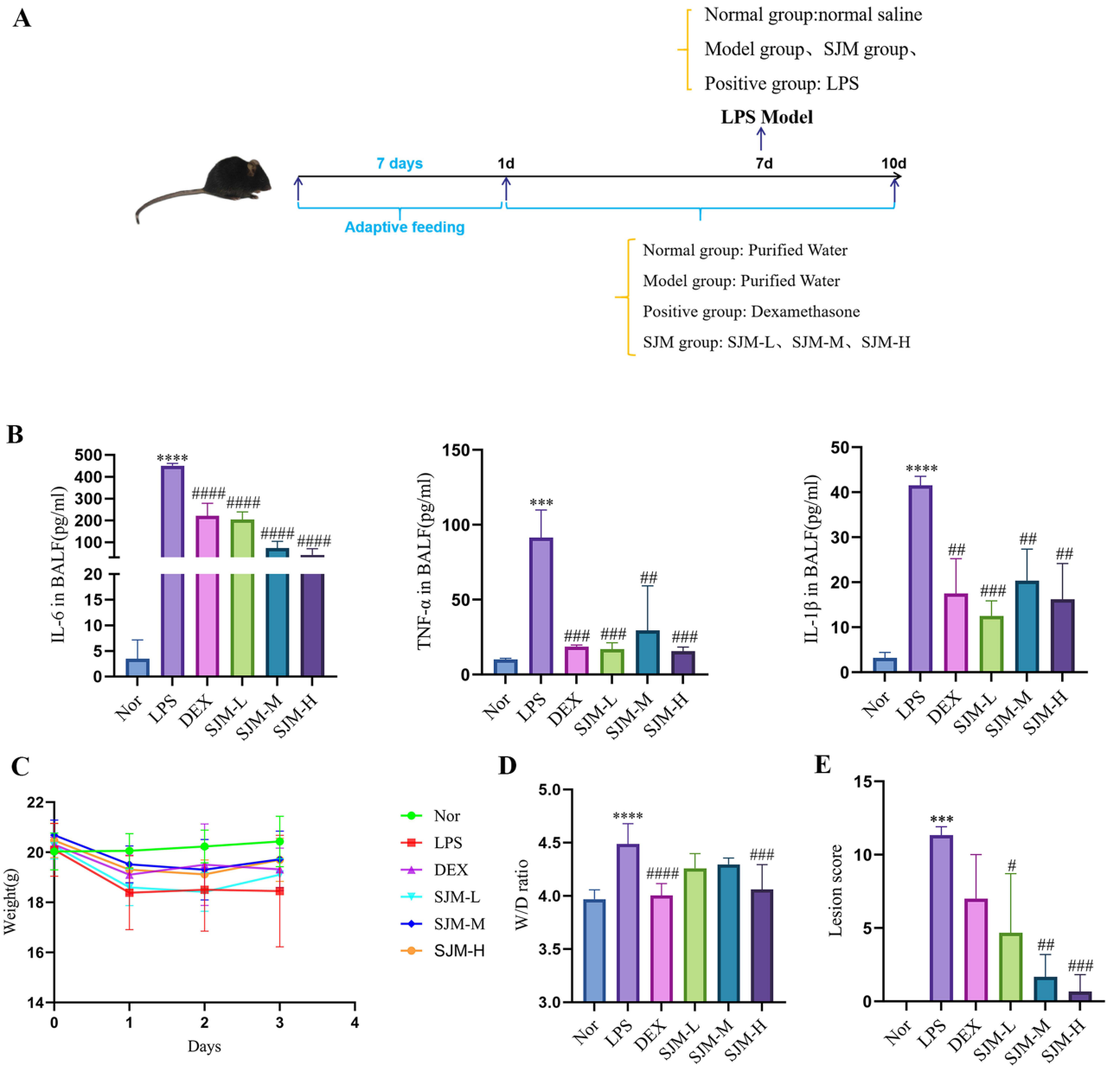

Figure 2 Continued.

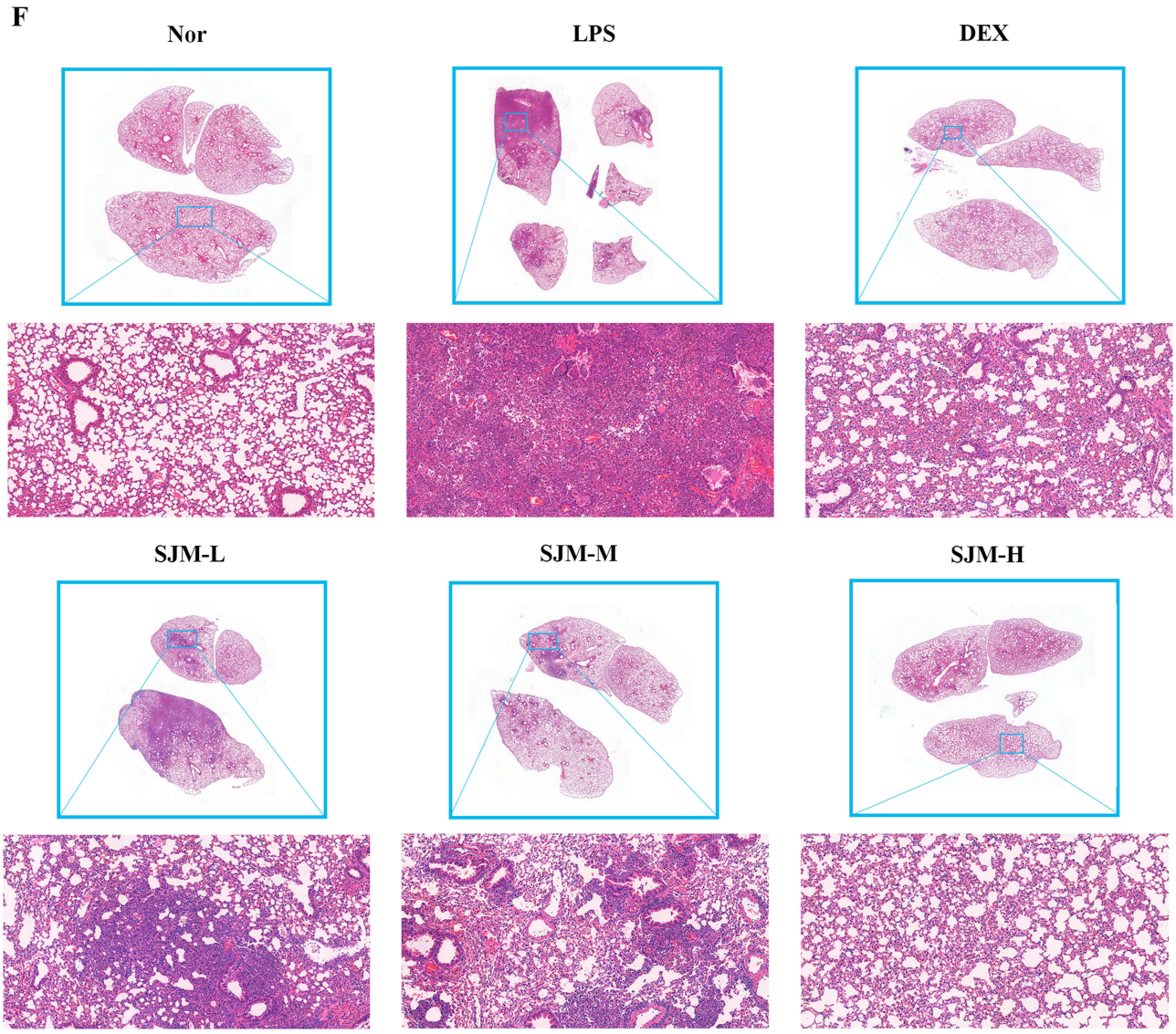

Figure 2 The protective effect of SJM on ALI induced by LPS in mice. (A) Development of animal models and the treatment process. (**B**) Comparison of the content levels of IL-6, IL-1β and TNF-α among different groups. (**C**) Curves of mouse weight changes. (**D**) W/D ratio. (**E–F**) Analysis results of HE staining of lung tissue. These data are represents as mean ± SD (n=7). ns P > 0.05. Compared with the control group ***p < 0.001, ****p < 0.0001; compared with the LPS group $^{\#}$p < 0.05, $^{\#\#}$p < 0.01, $^{\#\#\#}$p < 0.001, $^{\#\#\#\#}$p < 0.0001.

Through the analysis of the TNF and IL-17 pathways, it was concluded that JNK, P38, AP-1, C/EBPβ, IKKα, MMP3, and IKB-α might play crucial regulatory roles in modulating these pathways. We also conducted experimental verification for each of these key proteins (Figure 4A).

SJM Improves LPS-Induced Inflammation Through the IL-17 Signaling Pathway

WB analyses are presented in Figures 5A and B, which suggested the potential of SJM-H administration to significantly suppress the p-C/EBPβ, p-IKB-α expression. The immunofluorescence results demonstrated that the SJM-H administration could markedly reduce the IKKα, p-C/EBPβ, MMP3 levels (Figures 5C–F). Immunohistochemical results confirmed that the SJM-H treatment could significantly inhibit the MMP3 expression (Figures 5G and H).

https://doi.org/10.2147/JIR.S562152

SJM Improves LPS-Induced Inflammation Through the TNF Signaling Pathway

WB analyses are depicted in Figures 6A and B, revealing the potential of SJM-H administration to remarkably suppress the p-P38, p-JNK expression relative to the LPS administration. The immunofluorescence results demonstrated a notable C-JUN downregulation in the SJM-H group (Figure 6C). Immunohistochemical results confirmed that the SJM-H administration could significantly inhibit the C-JUN and C-FOS expression (Figure 6D).

Discussion

As an endotoxin, LPS can activate inflammatory cytokines, induce apoptosis, and cause barrier damage to alveolar epithelial cells, thereby contributing to the occurrence of ALI.[3] The ALI onset leads to widespread damage to both pulmonary alveolar epithelial and capillary endothelial cells,[16] causing a dysregulated intrapulmonary inflammatory response along with a diffuse infiltration of inflammatory cells throughout the lungs.[17] Apoptosis leads to the release of substantial inflammatory factors.[18] TNF-α acts on vascular endothelial cells, which is a primary inflammatory factor

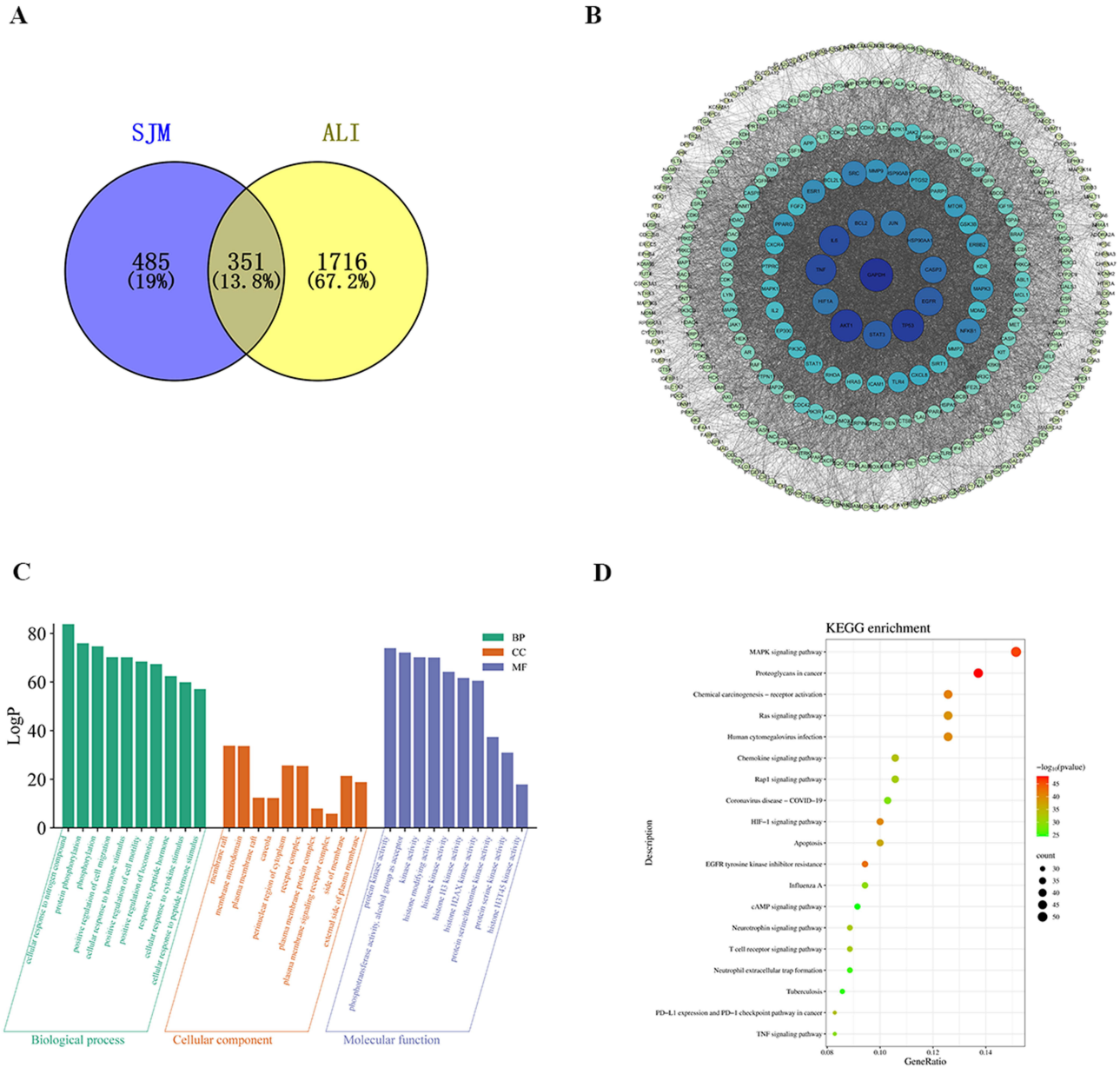

Figure 3 Continued.

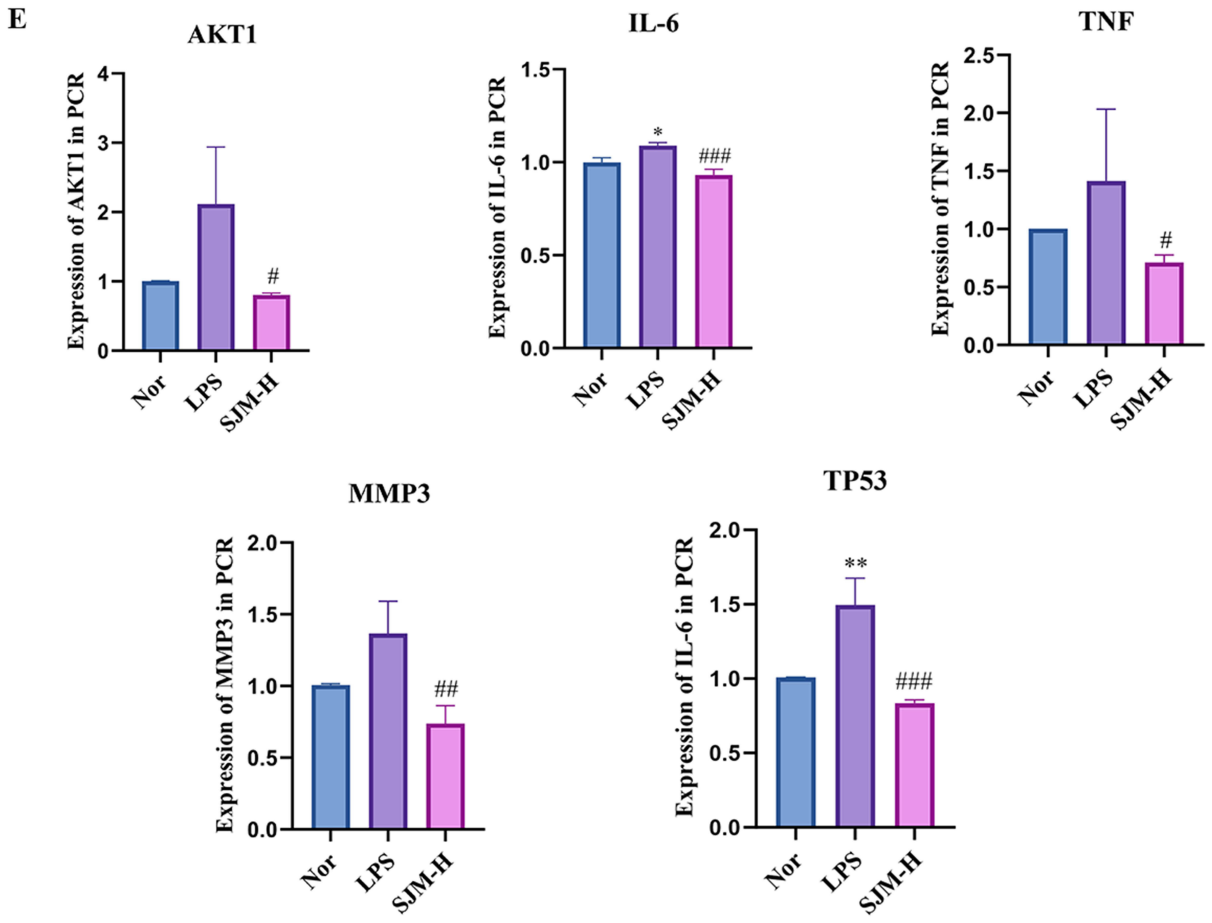

Figure 3 Network pharmacology analysis. (**A**):The Venny diagram of the active ingredient targets of SJM and the ALI targets. (**B**): PPI network diagram of SJM for the treatment of acute lung injury. (**C**): GO functional analysis of the intersection target of SJM. (**D**): KEGG pathway enrichment analysis of the intersection target of SJM. (**E**): Expression analysis of AKT, IL-6, TNF, MMP3, and TP53 mRNA in mouse serum. These data are represents as mean ± SD (n=3). ns $P > 0.05$. Compared with the control group $^{*}p < 0.05$,$^{**}p < 0.01$; compared with the LPS group $^{\#}p < 0.05$, $^{\#\#}p < 0.01$, $^{\#\#\#\#}p < 0.001$.

during the early phase of ALI.[19] This cytokine not only compromises the permeability of alveoli and capillaries but also activates inflammatory cells to release a range of inflammatory mediators, including IL-6 and IL-1β, thus aggravating the inflammatory cascade effect.[20] Our study explored how SJM influences the BALF IL-6, IL-1β, and TNF-α concentrations of mice, finding that SJM could notably inhibit the inflammatory response in ALI mice. The HE results also corroborated this finding, as the SJM administration group exhibited marked improvements in edema, hemorrhage, and inflammatory manifestations within lung tissue.

Although TCM lacks a specific nomenclature for ALI, it can be classified under the categories of "sudden asthma" and "wind-heat lung disease" based on its clinical manifestations such as cough, expectoration, shortness of breath, progressive respiratory difficulty, wheezing, cyanosis and other symptoms of lung qi congestion,[21,22] with the main pathogenesis being the invasion of the lungs by exogenous warm and toxic pathogens.[23,24] Relevant research indicates a definitive therapeutic efficacy of TCM on ALI.[25] The multiple TCM ingredients in the SJM have been proven to prevent ALI, with the flavonoids in *Houttuynia cordata* exerting their mechanism of action through the inhibition of TLR signaling and anti-inflammatory effects. Among the four main flavonoid glycosides in *Houttuynia cordata*, hyperoside and quercitrin contribute crucially to the therapeutic effect.[26] Platycodon grandiflorum exosome-like nanoparticles may influence polarization and inflammation of macrophages as a metabolic pathway (eg, glycolysis and lipid metabolism) modulator, thereby alleviating inflammation and aiding in lung repair.[27] *Forsythiae Fructuse* exhibits anti-inflammatory effects and safeguards the lung and intestinal epithelial barriers by regulating PPAR-γ/RXR-α in LPS-induced ALI.[8] The leaves of *Perilla frutescens* can inhibit LPS-induced murine ALI by suppressing the KAT2A expression, demonstrating a

https://doi.org/10.2147/JIR.S562152

dose-dependent anti-inflammatory effect.[28] The extract of Chrysanthemum protects mice from the LPS-induced ALI as a toll-like receptor 4 pathway regulator.[29] The effective component database in SJM was determined by LC-MS, identifying the corresponding TCM chemical components, and further clarifying the components that could exert an effect on ALI. Moreover, a decomposition pathway analysis was conducted on the representative components, with their chemical structures being distinctly identified. It has been clearly demonstrated that the phloroglucinol acid has an improving effect on ALI. Chlorogenic acid alleviates inflammation and ameliorates LPS-induced ALI by suppressing the expression of KAT2A.[30] Besides, chlorogenic acid targeting TLR4/3 alleviates oxidative stress-mediated NLRP3/NF-κB axis, thereby improving the ARDS induced by LPS + POLY I:C.[31] Rutin improves LPS-induced murine ALI as a cGAS-STING-NLRP3 axis inhibitor[32] Luteolin alleviates ALI through its immunomodulatory effects on the BTK and FLT3 signaling pathways and by exerting anti-lung necrosis effects.[33] The saponins from *Platycodon grandiflorum* demonstrate significant liver-protective properties against the APAP-induced ALI, mainly via the NF-κB and AMPK/PI3K/Akt systems.[34] The above results collectively indicate that SJM possesses heat-clearing and detoxifying properties, which achieves ALI treatment through the synergistic action of multiple components.

By integrating transcriptomic analysis techniques, the key signaling pathways of SJM in the ALI context were identified as the IL-17 and the TNF. These two pathways can partake in systemic inflammatory responses and play significant roles in pulmonary inflammatory diseases. Macrophages serve as the primary source of TNF-α in the pulmonary region.[35] Activation of the above two key pathways is intricately linked to apoptosis and can concurrently activate the downstream MAPK, NF-κB pathways, thereby contributing to the apoptosis process regulation and resulting in comprehensive lung tissue damage.[36–38] The first pathway derived from the network pharmacology KEGG analysis was MAPK, aligning with the results of transcriptome sequencing. In our experiment, WB, immunofluorescence, and immunohistochemistry were employed to verify that SJM can inhibit the expression of key proteins P-P38, P-IKBα, IKKα, P-C/EBPβ, P-JNK, C-JUN, C-FOS, IKK-α and MMP3 within the two identified key pathways, thereby reducing

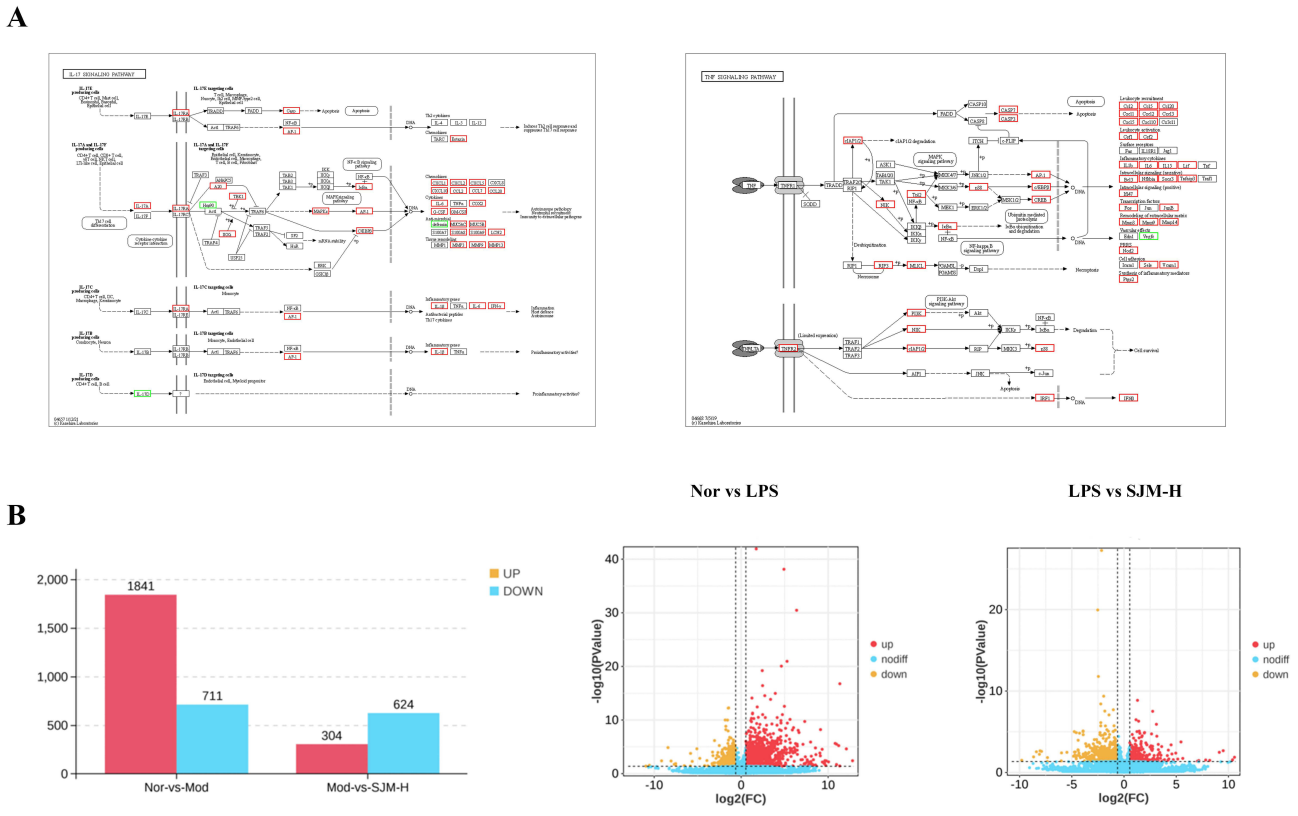

Figure 4 Continued.

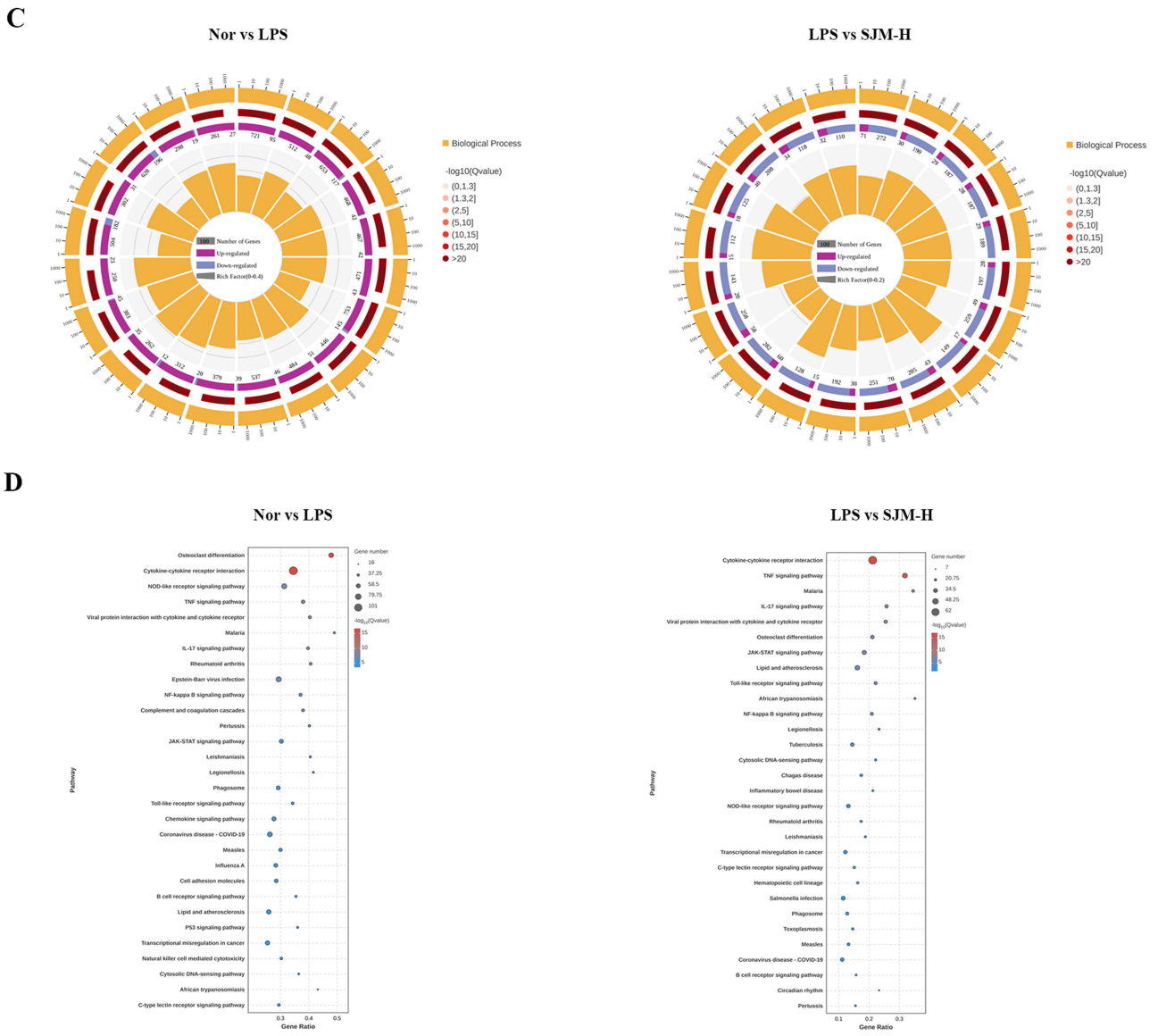

Figure 4 Transcriptomic analysis of the lung tissue of SJM-H group in mice. (**A**) The key pathway map obtained through KEGG enrichment analysis: TNF signal pathway and IL-17 signal pathway. (**B**) Statistical analysis of the different gene data expressed between groups. (**C**) GO functional analysis of the different gene data. (**D**) KEGG enrichment analysis of the different gene data.

the expression of pertinent apoptosis proteins downstream and achieving the effect of inhibiting ALI (Figure 7). P38 belongs to the MAPK family. Various inflammatory factors and other signals can activate the TNF signaling pathway.[39] Inhibiting the expression of downstream P-C/EBPβ leads to the progressive amplification of extracellular signal stimulation, along with the signal transmission to the nucleus, achieving the expression regulation of target genes. Previously, there were few reports concerning C/EBPβ in relation to ALI. Our investigation clarified through WB and immunofluorescence methods that SJM can significantly inhibit the expression of P-C/EBPβ, consequently regulating the secretion and expression of inflammatory factors and related proteins.

In recent years, given the rising incidence of respiratory system diseases, ALI has emerged as a focal point of research, particularly regarding anti-ALI mechanism. In the inflammatory response triggered by ALI, the macrophage regulation plays a crucial role. A recent study has proposed a fresh approach for treating ALI and inflammatory-related conditions by regulating the metabolism of macrophages. It indicates that stigmasterol may facilitate mCa^{2+} uptake by

https://doi.org/10.2147/JIR.S562152

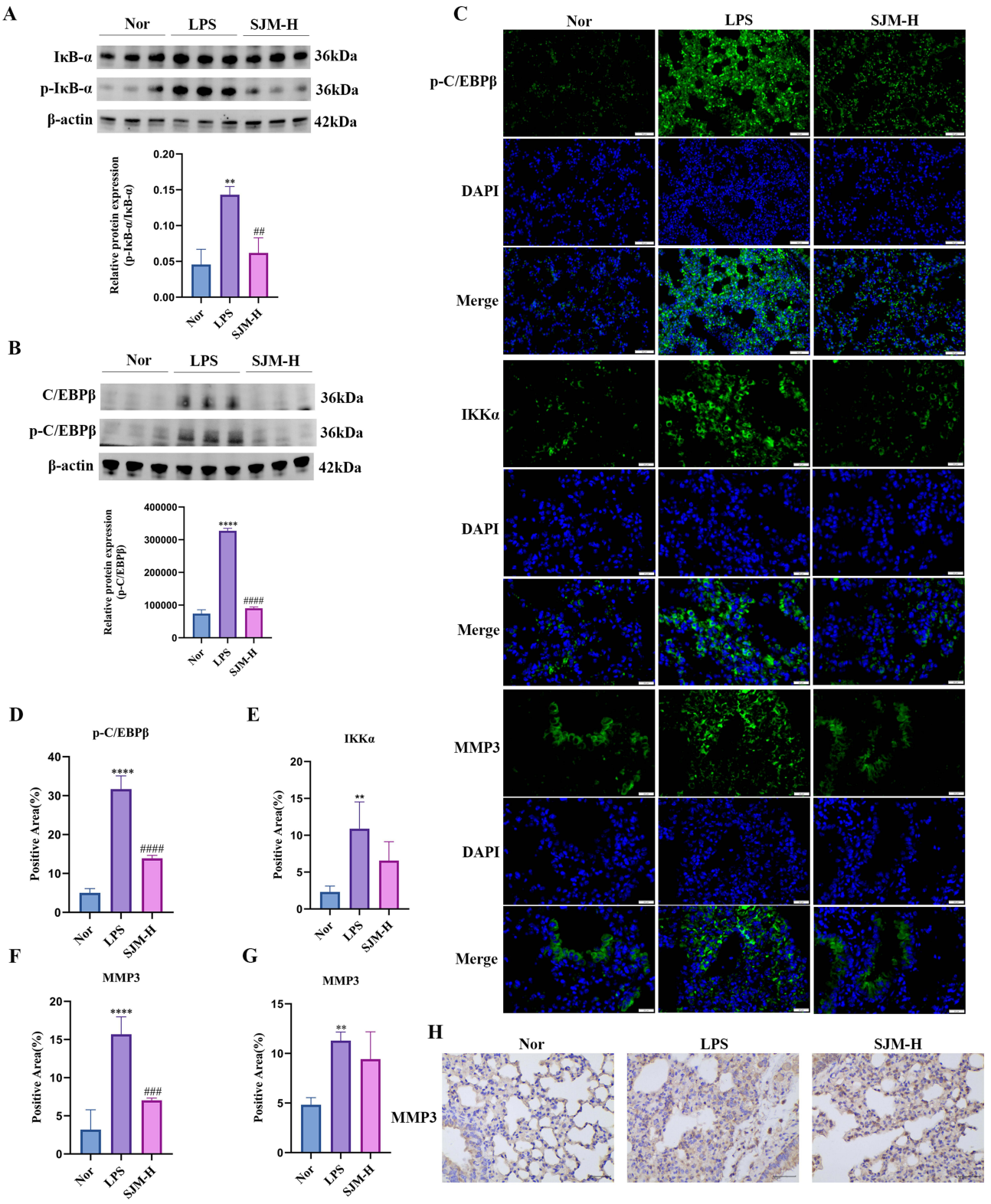

Figure 5 The inhibitory effect of SJM-H on the IL-17 signal pathway. (**A**) Western blotof IκB-α, p-IκB-α and protein expression levels of p-IκB-α/IκB-α. (**B**) Western blot of C/EBPβ, p-C/EBPβ and protein expression levels of p-C/EBPβ. (**C**) Immunofluorescence detection of p-C/EBPβ, IKKα and MMP3 in the lungs of mice after DAPI staining. Scale: 50 μm.(**D**–**F**) The calculation result of the proportion of the positive area in the lung tissue. (**G** and **H**) Expression of MMP3 immunohistochemistry and calculation of positive area. Scale: 50 μm. These data are represents as mean ± SD (n=3). ns P > 0.05. Compared with the control group **p < 0.01, ****p < 0.0001; compared with the LPS group $^{\#\#}$p < 0.01, $^{\#\#\#\#}$p < 0.001, $^{\#\#\#\#\#}$p < 0.0001.

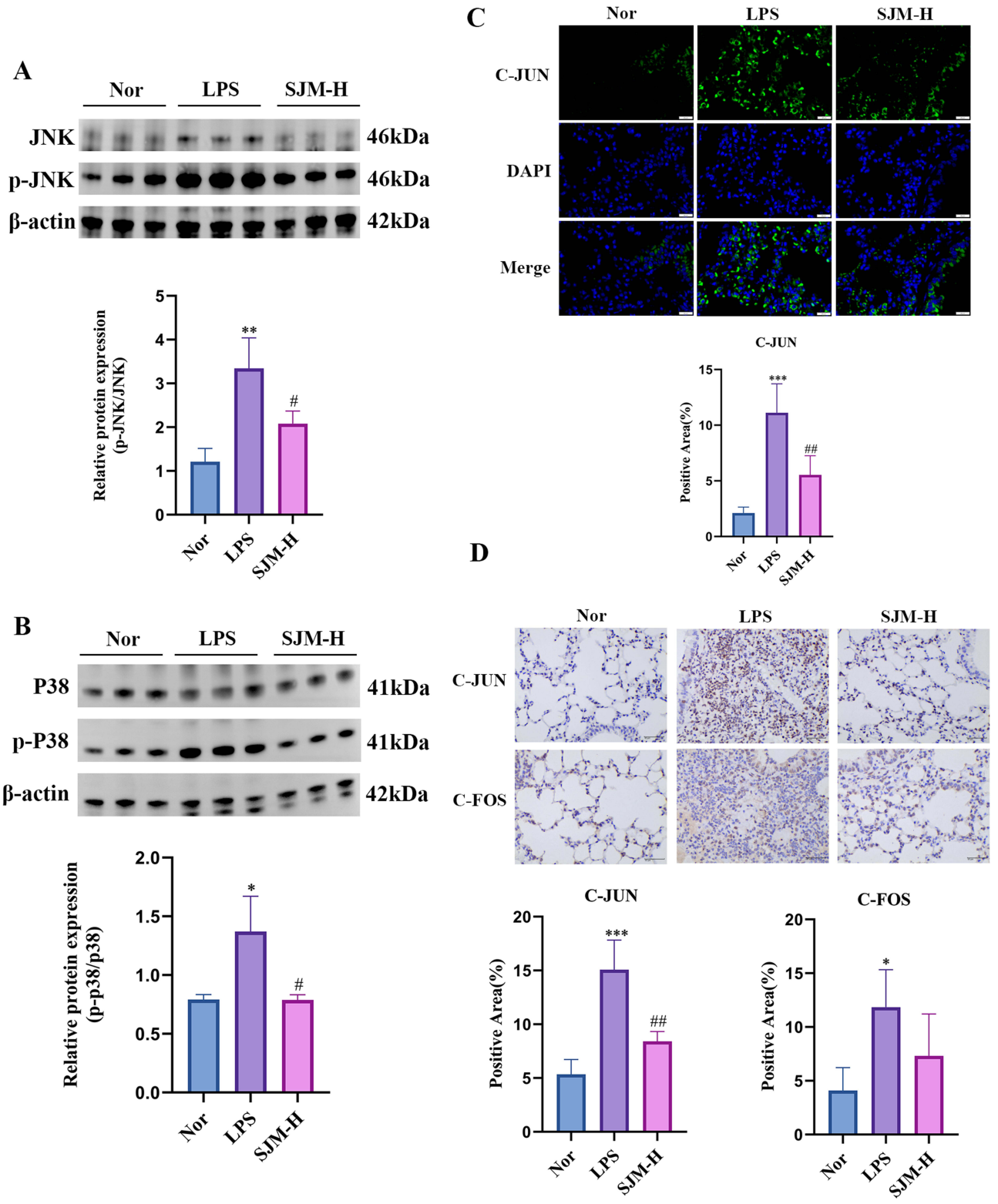

Figure 6 The inhibitory effect of SJM-H on the TNF signal pathway. (**A**) Western blot of JNK, p-JNK and protein expression levels of p-JNK/JNK. (**B**) Western blot of P38, p-P38 and protein expression levels of p-P38/P38. (**C**) Immunofluorescence detection of C-JUN in the lungs of mice after DAPI staining. Scale: 50 μm. (**D**) Expression of C-JUN, C-FOS immunohistochemistry and calculation of positive area.Scale: 50 μm. These data are represents as mean ± SD (n=3). ns $P > 0.05$. Compared with the control group $^{*}p < 0.05$, $^{**}p < 0.01$, $^{***}p < 0.001$; compared with the LPS group $^{\#}p < 0.05$, $^{\#\#}p < 0.01$.

https://doi.org/10.2147/JIR.S562152

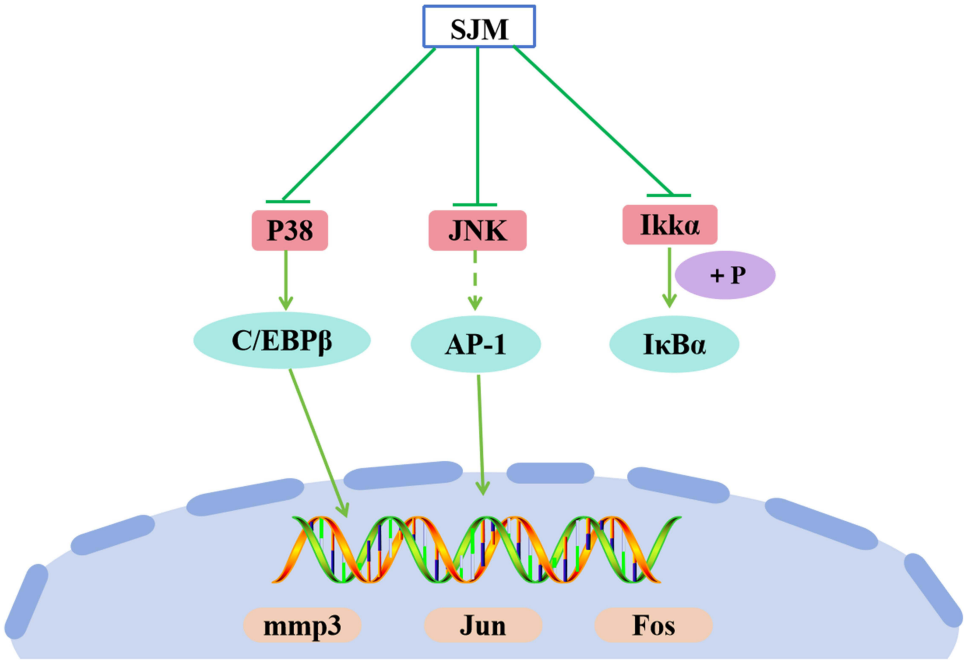

Figure 7 Mechanism of SJM in the alleviation of ALI. "⊣" means SJM can inhibit P38, JNK, IKKα, "→" means downstream genes of P38, JNK, and IKKα.

upregulating MCU expression, and through the mCa^{2+}/PDP1/PDH signaling system, this compound can inhibit the polarization of inflammatory pulmonary macrophages while regulating their metabolic prcesses[40] During the onset of ALI, the compromise of alveolar–capillary barrier integrity can directly result in ALI. Extensive research has been conducted concerning the functions of extracellular vesicles (EVs) in regulating cellular inflammation alongside injury responses, and their effects on the dysfunction of pulmonary endothelial, epithelial cells, alveolar neutrophils and macrophages linked to the potential onset of pneumonia and ALI/ARDS damage. EV-based ionizing radiation exhibits considerable promise in mitigating lung damage and thereby preventing the ALI/ARDS.[1] Future experimental research of SJM will focus on the regulation of macrophages and the mechanism by which EVs can ameliorate cell damage and alleviate ALI.

Conclusions

In conclusion, our study indicates that SJM can successfully inhibit the inflammation and damage resulting from LPS-induced ALI. The mechanism of its action may involve the IL-17 and TNF signaling suppression. This model robustly and reproducibly recapitulates the cardinal features of ALI. These features include LPS directly injures the alveolar epithelium and leading to pulmonary edema. This model induces a strong pro-inflammatory response, with significant elevation of cytokines, which are also critically implicated in human ALI. Therefore, we conclude that SJM has therapeutic potential when used in clinical settings for ALI. At present, this study has not conducted experiments on the pharmacological effects and mechanisms of cells. In the future, cell research will be carried out.

Abbreviations

SJM, Siji Kangbingdu Mixture; ALI, Acute lung injury; TCM, Traditional Chinese Medicine; LPS, Lipopolysaccharide; ARDS, Acute respiratory distress syndrome; LC-MS, Liquid Chromatography-Mass Spectrometry; UHPLC-Q-Orbitrap HRMS, Ultra-High-Performance Liquid Chromatography coupled with Quadrupole-Orbitrap High Resolution Mass Spectrometry; WB, Western Blotting; W/D, Wet/Dry; BALF, Bronchoalveolar Lavage Fluid; GO, Gene ontology; KEGG, Kyoto Encyclopedia of Genes and Genomes; H&E, hematoxylin and eosin; MF, molecular function; BP, biological process; CC, cellular component.

Data Sharing Statement

The data are available from the corresponding author upon reasonable request.

Author Contributions

All authors made a significant contribution to the work reported, whether that is in the conception, study design, execution, acquisition of data, analysis and interpretation, or in all these areas. Every author took part in drafting, revising or critically reviewing the article; gave final approval of the version to be published; have agreed on the journal to which the article has been submitted; and agree to be accountable for all aspects of the work. Yuan Wang, Writing-original draft, Data curation; Huiying Zhou, Writing-review and editing, Validation; Bo Wang, Methodology, Software, Writing – review and editing; Yuxi Liu, Investigation, Formal analysis, Writing – review and editing; Kaihua Long, Conceptualization, Project administration, Writing – review and editing; Hong Zhang, Funding acquisition, Validation, Writing – review and editing.

Funding

Science and Technology Project of Xi'an City (23CXLHTJSGG0004-2023); Key Research Project of Shaanxi Province (2024SF-YBXM-489); Young Talent Support Program of Shaanxi Provincial Federation of Science and Technology (20230321); Project of Quality Control and Innovation Research on Traditional Chinese Medicine of Shaanxi Provincial Administration of Traditional Chinese Medicine (SZY-KJCYC-2025-ZY-006); Research and Innovation Team for Quality Control and Innovation of Qin Medicine; Projects of Shaanxi Academy of Traditional Chinese Medicine (Shaanxi Provincial Hospital of Traditional Chinese Medicine) (2025-42, 2025-17).

Disclosure

The authors declare no conflicts of interest.

References

1. Hu Q, Zhang S, Yang Y, et al. Extracellular vesicles in the pathogenesis and treatment of acute lung injury. *Mil Med Res*. 2022;9(1):61. doi:10.1186/s40779-022-00417-9
2. Ma A, Feng Z, Li Y, et al. Ferroptosis-related signature and immune infiltration characterization in acute lung injury/acute respiratory distress syndrome. *Respir Res*. 2023;24(1):154. doi:10.1186/s12931-023-02429-y
3. Meng M, Huo R, Wang Y, et al. Lentinan inhibits oxidative stress and alleviates LPS-induced inflammation and apoptosis of BMECs by activating the Nrf2 signaling pathway. *Int J Biol Macromol*. 2022;222(Pt B):2375–2391. doi:10.1016/j.ijbiomac.2022.10.024
4. Yang HH, Duan JX, Liu SK, et al. A COX-2/sEH dual inhibitor PTUPB alleviates lipopolysaccharide-induced acute lung injury in mice by inhibiting NLRP3 inflammasome activation. *Theranostics*. 2020;10(11):4749–4761. doi:10.7150/thno.43108
5. Zhang J, Guo Y, Mak M, Tao Z. Translational medicine for acute lung injury. *J Transl Med*. 2024;22(1):25. doi:10.1186/s12967-023-04828-7
6. Fan Y, Liu W, Wan R, et al. Efficacy and safety of yinqiao powder combined with western medicine in the treatment of pneumonia: a systematic review and meta-analysis. *Complement Ther Clin Pract*. 2021;42:101297. doi:10.1016/j.ctcp.2020.101297
7. Li J, Hu YP, Liang XL, Liu MW. Sodium houttuyniae attenuates ferroptosis by regulating TRAF6-c-Myc signaling pathways in lipopolysaccharide-induced acute lung injury (ALI). *BMC Pharmacol Toxicol*. 2024;25(1):63. doi:10.1186/s40360-024-00787-x
8. Wang J, Luo L, Zhao X, et al. Forsythiae Fructuse extracts alleviates LPS-induced acute lung injury in mice by regulating PPAR-γ/RXR-α in lungs and colons. *J Ethnopharmacol*. 2022;293:115322. doi:10.1016/j.jep.2022.115322
9. Liu G, Zheng Q, Pan K, Xu X. Protective effect of Chrysanthemum morifolium Ramat. ethanol extract on lipopolysaccharide induced acute lung injury in mice. *BMC Complement Med Ther*. 2020;20(1):235. doi:10.1186/s12906-020-03017-z
10. Sum CH, Li TW, Zhang H, et al. Assessing the efficacy and safety of Yinqiao powder-maxing Ganshi decoction in the treatment of the major symptoms of mild and moderate COVID-19 by telemedicine-study protocol for a randomized, double-blind, placebo-controlled trial. *Front Pharmacol*. 2024;14:1261338. doi:10.3389/fphar.2023.1261338
11. Ma Z, Yin Z, Wei G, et al. Traditional Chinese medicine treatment plan for COVID-19 in Shaanxi province (Trial version 2). *Shaanxi Journal of Traditional Chinese Medicine*. 2020;41(03):275–277.(Chinese.
12. Kilkenny C, Browne W, Cuthill IC, Emerson M, Altman DG. Animal research: reporting in vivo experiments: the ARRIVE guidelines. *Br J Pharmacol*. 2010;160(7):1577–1579. doi:10.1111/j.1476-5381.2010.00872.x
13. D'Alessio FR. Mouse models of acute lung injury and ARDS. *Methods Mol Biol*. 2018;1809:341–350. doi:10.1007/978-1-4939-8570-8_22
14. Chen H, Bai C, Wang X. The value of the lipopolysaccharide-induced acute lung injury model in respiratory medicine. *Expert Rev Respir Med*. 2010;4(6):773–783. doi:10.1586/ers.10.71
15. Zhang M, Shang L, Zhou F, et al. Dachengqi decoction dispensing granule ameliorates LPS-induced acute lung injury by inhibiting PANoptosis in vivo and in vitro. *J Ethnopharmacol*. 2025;336:118699. doi:10.1016/j.jep.2024.118699
16. Li J, Deng SH, Li J, et al. Obacunone alleviates ferroptosis during lipopolysaccharide-induced acute lung injury by upregulating Nrf2-dependent antioxidant responses. *Cell Mol Biol Lett*. 2022;27(1):29. doi:10.1186/s11658-022-00318-8

17. Long ME, Mallampalli RK, Horowitz JC. Pathogenesis of pneumonia and acute lung injury. *Clin Sci (Lond)*. 2022;136(10):747–769. doi:10.1042/CS20210879
18. Lu Q, Huang S, Meng X, et al. Mechanism of phosgene-induced acute lung injury and treatment strategy. *Int J Mol Sci*. 2021;22(20):10933. doi:10.3390/ijms222010933
19. Jiao Y, Zhang T, Zhang C, et al. Exosomal miR-30d-5p of neutrophils induces M1 macrophage polarization and primes macrophage pyroptosis in sepsis-related acute lung injury. *Crit Care*. 2021;25(1):356. doi:10.1186/s13054-021-03775-3
20. Zhu J, Zhou J, Feng B, et al. MSCs alleviate LPS-induced acute lung injury by inhibiting the proinflammatory function of macrophages in mouse lung organoid-macrophage model. *Cell Mol Life Sci*. 2024;81(1):124. doi:10.1007/s00018-024-05150-1
21. Ding Z, Zhong R, Yang Y, et al. Systems pharmacology reveals the mechanism of activity of Ge-Gen-Qin-Lian decoction against LPS-induced acute lung injury: a novel strategy for exploring active components and effective mechanism of TCM formulae. *Pharmacol Res*. 2020;156:104759. doi:10.1016/j.phrs.2020.104759
22. Lu Y, Wu Y, Huang M, et al. Fuzhengjiedu formula exerts protective effect against LPS-induced acute lung injury via gut-lung axis. *Phytomedicine*. 2024;123:155190. doi:10.1016/j.phymed.2023.155190
23. Chen P, Lin C, Jin Q, et al. Investigating mechanisms of Sophora davidii (Franch.) skeels flower extract in treating LPS-induced acute pneumonia based on network pharmacology. *J Ethnopharmacol*. 2025;337(Pt 2):118914. doi:10.1016/j.jep.2024.118914
24. Xie L, Zhang G, Wu Y, et al. Protective effects of Wenqingyin on sepsis-induced acute lung injury through regulation of the receptor for advanced glycation end products pathway. *Phytomedicine*. 2024;129:155654. doi:10.1016/j.phymed.2024.155654
25. Liu Y, Wang X, Chen Y, et al. Pharmacological mechanisms of traditional Chinese medicine against acute lung injury: from active ingredients to herbal formulae. *Phytomedicine*. 2024;135:155562. doi:10.1016/j.phymed.2024.155562
26. Ling LJ, Lu Y, Zhang YY, et al. Flavonoids from houttuynia cordata attenuate H1N1-induced acute lung injury in mice via inhibition of influenza virus and toll-like receptor signalling. *Phytomedicine*. 2020;67:153150. doi:10.1016/j.phymed.2019.153150
27. Fu J, Liu Z, Feng Z, et al. Platycodon grandiflorum exosome-like nanoparticles: the material basis of fresh platycodon grandiflorum optimality and its mechanism in regulating acute lung injury. *J Nanobiotechnology*. 2025;23(1):270. doi:10.1186/s12951-025-03331-z
28. Guo J, Zhang Y, Du Y, et al. Perilla frutescens leaf extracts alleviate acute lung injury in mice by inhibiting KAT2A. *J Ethnopharmacol*. 2025;336:118730. doi:10.1016/j.jep.2024.118730
29. Wu XL, Feng XX, Li CW, et al. The protective effects of the supercritical-carbon dioxide fluid extract of chrysanthemum indicum against lipopolysaccharide-induced acute lung injury in mice via modulating toll-like receptor 4 signaling pathway. *Mediators Inflamm*. 2014;2014:246407. doi:10.1155/2014/246407
30. Lv B, Guo J, Du Y, et al. Chlorogenic acid reduces inflammation by inhibiting the elevated expression of KAT2A to ameliorate lipopolysaccharide-induced acute lung injury. *Br J Pharmacol*. 2023;180(16):2156–2171. doi:10.1111/bph.16069
31. Jain S, Saha P, Syamprasad NP, et al. Targeting TLR4/3 using chlorogenic acid ameliorates LPS+POLY I:C-induced acute respiratory distress syndrome via alleviating oxidative stress-mediated NLRP3/NF-κB axis. *Clin Sci (Lond)*. 2023;137(10):785–805. doi:10.1042/CS20220625
32. Zhou X, Wang Z, Wang Y, et al. Rutin ameliorates LPS-induced acute lung injury in mice by inhibiting the cGAS-STING-NLRP3 signaling pathway. *Front Pharmacol*. 2025;16:1590096. doi:10.3389/fphar.2025.1590096
33. Cao Z, Rao H, Yang W, et al. Luteolin mitigates acute lung injury through immune modulation and antinecroptosis effects by targeting the BTK and FLT3 signaling pathways. *J Agric Food Chem*. 2025;73(9):5180–5193. doi:10.1021/acs.jafc.4c06704
34. Leng J, Wang Z, Fu CL, et al. NF-κB and AMPK/PI3K/Akt signaling pathways are involved in the protective effects of platycodon grandiflorum saponins against acetaminophen-induced acute hepatotoxicity in mice. *Phytother Res*. 2018;32(11):2235–2246. doi:10.1002/ptr.6160
35. Sun J, Liao Z, Li Z, et al. Down-regulation miR-146a-5p in schwann cell-derived exosomes induced macrophage M1 polarization by impairing the inhibition on TRAF6/NF-κB pathway after peripheral nerve injury. *Exp Neurol*. 2023;362:114295. doi:10.1016/j.expneurol.2022.114295
36. Chen X, Tang J, Shuai W, Meng J, Feng J, Han Z. Macrophage polarization and its role in the pathogenesis of acute lung injury/acute respiratory distress syndrome. *Inflamm Res*. 2020;69(9):883–895. doi:10.1007/s00011-020-01378-2
37. Xiao K, He W, Guan W, et al. Mesenchymal stem cells reverse EMT process through blocking the activation of NF-κB and Hedgehog pathways in LPS-induced acute lung injury. *Cell Death Dis*. 2020;11(10):863. doi:10.1038/s41419-020-03034-3
38. Wang Y, Wang Y, Ma J, et al. YuPingFengSan ameliorates LPS-induced acute lung injury and gut barrier dysfunction in mice. *J Ethnopharmacol*. 2023;312:116452. doi:10.1016/j.jep.2023.116452
39. Xu Y, Zhang C, Cai D, Zhu R, Cao Y. Exosomal miR-155-5p drives widespread macrophage M1 polarization in hypervirulent Klebsiella pneumoniae-induced acute lung injury via the MSK1/p38-MAPK axis. *Cell Mol Biol Lett*. 2023;28(1):92. doi:10.1186/s11658-023-00505-1
40. Bao-Yuan H, Shu-Ru L, Le-Xin C, et al. Shikonin ameliorated LPS-induced acute lung injury in mice via modulating MCU-mediated mitochondrial Ca2+ and macrophage polarization. *Phytomedicine*. 2024;135:156043. doi:10.1016/j.phymed.2024.156043